COMPARISON OF THE 2D AND 3D ANALYSES METHODS FOR CFRDS

A THESIS SUBMITTED TO
THE GRADUATE SCHOOL OF NATURAL AND APPLIED SCIENCES
OF
MIDDLE EAST TECHNICAL UNIVERSITY

BY

HALİL FIRAT ÖZEL

IN PARTIAL FULFILLMENT OF THE REQUIREMENTS
FOR
THE DEGREE OF MASTER OF SCIENCE
IN
CIVIL ENGINEERING

SEPTEMBER 2012

Approval of the thesis:

COMPARISON OF THE 2D AND 3D ANALYSES METHODS FOR CFRDS

submitted by **HALİL FIRAT ÖZEL** in partial fulfillment of the requirements for the degree of **Master of Science in Civil Engineering Department, Middle East Technical University** by,

Prof. Dr. Canan Özgen _____
Dean, Graduate School of **Natural and Applied Sciences**

Prof. Dr. Güney Özcebe _____
Head of Department, **Civil Engineering**

Assist. Prof. Dr. Yalın Arıcı _____
Supervisor, **Civil Engineering Dept., METU**

Examining Committee Members

Prof. Dr. Melih Yanmaz _____
Civil Engineering Dept., METU

Assist. Prof. Dr. Yalın Arıcı _____
Civil Engineering Dept., METU

Prof . Dr. M. Yener Özkan _____
Civil Engineering Dept., METU

Assoc. Prof. Dr. Afşin Sarıtaş _____
Civil Engineering Dept., METU

Altuğ Akman, M.Sc _____
General Manager Asistant, ES PROJE Eng.and Consulting

Date: 20.09.2012

I hereby declare that all information in this document has been obtained and presented in accordance with academic rules and ethical conduct. I also declare that, as required by these rules and conduct, I have fully cited and referenced all material and results that are not original to this work.

Name, Last name :Halil Fırat ÖZEL

Signature :

ABSTRACT

COMPARISON OF THE 2D AND 3D ANALYSES METHODS FOR CFRDS

ÖZEL, Halil Fırat

M.Sc., Department of Civil Engineering

Supervisor : Assist. Prof. Dr. Yalın ARICI

September 2012, 81 Pages

The purpose is to compare the 2D and 3D analysis methodologies in investigating the performance of a Concrete Faced Rockfill Dam (CFRD) under static and dynamic loading conditions. Çokal Dam is the case study which is a CFRD located in northwest Turkey at the Thracian Peninsula. Rockfill interface and faceplate were simulated as nonlinear modulus of elasticity, detailed nonlinear tractive behavior and total strain rotating crack model, respectively. These behaviors were calibrated to define the exact behavior by detailed material tests. The analyses that cannot be done by 2D analyses, such as stress, crack width distribution along the face slab are conducted by 3D analyses to determine the necessity of these outcomes. Since effect of valley ends cannot be produced by 2D analyses, it is necessary to check 3D analyses to ensure liability of the results. Another comparison between detailed analysis of 2D models and linear elastic 2D models were covered to get practical and industrial solutions for the guiding methods of CFRDs for preliminary designs in this study.

Keywords: CFRD, 2 and 3D analyses, static and dynamic loading, guiding methods

ÖZ

ÖYBKDBLER İÇİN 2 VE 3 BOYUTLU ANALİZ YÖNTEMLERİNİN KARŞILAŞTIRILMASI

ÖZEL, Halil Fırat
Yüksek Lisans, İnşaat Mühendisliği Bölümü
Tez Yöneticisi : Yard. Doç. Dr. Yalın ARICI
Eylül 2012, 81 Sayfa

Amaç, statik ve dinamik yükleme koşulları altında bir Ön Yüzü Beton Kaplı Kaya Dolgu Barajı'nın (ÖYBKDB) performansının araştırılması için 2 ve 3B analiz metodlarının karşılaştırılmasıdır. Bu çalışmada örnek alınan baraj Çokal Barajıdır. Çokal Barajı Türkiye'nin kuzeybatısında Trakya Yarımadası'nda yer alan bir ön yüzü beton kaplı kaya dolgu barajıdır. Kaya dolgu, arayüz ve ön yüz plakası sırasıyla, nonlineer elastisite modülü ve detaylı doğrusal olmayan gerilme ve toplam gerilme dönen çatlak modeli olarak simüle edilmiştir. Bu davranışlar ayrıntılı malzeme testleri ile kesin davranışını tanımlamak için kalibre edilmiştir. İki boyutlu analizlerde elde edilmesi mümkün olmayan sonuçlar, örneğin ön yüz plakası boyunca oluşan gerilim ve çatlak genişilği dağılımı, üç boyutlu analizlerce yapılıp, gerekliliğinin önemi araştırılmıştır. Vadi sonunun etkisi iki boyutlu analizlerde elde etmenin mümkün olmadığından bu kontrolün yapılması gerekmiştir. ÖYBKDB modellemelerinde pratik ve endüstriyel çözümler oluşturmak için bu çalışmada iki boyutlu detaylı analizler ile doğrusal elastik modellerin karşılaştırılması yapılarak ön tasarımda kullanılmak üzere kılavuz yöntemler geliştirilmiştir.

Anahtar Kelimeler: ÖYBKDB, 2 ve 3B analizler, statik ve dinamik yükleme, kılavuz yöntem

To My Family

ACKNOWLEDGEMENTS

The author wishes to express his utmost gratitude to his supervisor Assist. Prof. Dr. Yalın ARICI for his guidance, advice, criticism, encouragements and insight throughout the research.

Prof. Dr. Barış BİNİCİ is also sincerely acknowledged for his valuable support.

The author is grateful for all continuous support, understanding and encouragement he has received from his family and friends.

This study has been conducted with the funding provided by The Scientific and Technological Research Council of Turkey (TUBITAK) under the grant MAG108M491.

TABLE OF CONTENTS

LIST OF TABLES

TABLES

LIST OF FIGURES

FIGURES

CHAPTER 1

INTRODUCTION AND GENERAL REVIEW OF THE CASE STUDY

1.1 INTRODUCTION

The construction of the concrete faced rockfill dams (CFRD) is rapid and easy in contrast to the building of clay core earth fill dams rendering them extremely popular in developing countries. Usage of 2D analyses methods for the estimation of settlements and the prediction of structural stability is common procedure for the design of embankment dams. Similar procedures have been used for the design of CFRDs, usually underestimating the fact that CFRD systems present a different challenge compared to an earth-fill dam due to the use of a reinforced concrete face plate as the major water retaining element. This common approach did not cause any problems for smaller dams, however, for higher dams, cracking of the face plate led to significant problems in the performance of the dam (Sobrinho et al., 2007, Pinto, 2007, Johannesson and Tohlang, 2007, Chen and Han, 2009). The contact surface between the face plate and the embankment causing interaction between them leads to cracking on a face plate, and that requires a 3D investigation due to the nature of the problem. That's why the solution cannot be handled by conventional plane-strain analysis techniques.

The comparisons of the performance of embankments in 2 and 3D analysis techniques were covered extensively in (Gazetas, 1987). However, the amount of the studies on the computer models and estimation of the CFRD performance using 3D finite element techniques is very limited. An analytical study (Boulanger et al., 1995)

conducted on the modeling of the embankment of a CFRD comparing two recorded motions on the system with the simulation results. The 3D modeling of the Jinxia and ZipingPu CFRDs are provided in studies of Zhang et al. (2007, 2009) with rigorous modeling of the fill albeit with the elastic modeling of the face plate. As the recent failures in CFRDs showed that nonlinear action in the face plate can indeed be critical, in contrast to the previous authors, the focus of this work is chosen as the investigation of the cracking of the face plate of a CFRD 3D modeling. The primary goals of this study are 1) to determine the possible failure mechanisms of a CFRD for earthquake excitation 2) to investigate the significance of the 3D modeling to determine the performance of the face plate 3) to compare the results of 2D and 3D analysis on a CFRD with a focus on the plate performance.

The analysis of the performance of a CFRD requires not only the rigorous modeling of the face plate and the rockfill behavior but also the simulation of the complex sliding/opening response at the vertical construction joints, between the cushion layer-face plate and the face plate-plinth base. A total strain based crack model with embedded reinforcements was used to predict the crack development for the reinforced concrete face plate for the case study utilized, the Çokal Dam. The pressure dependent mechanical response of the rockfill underlying the face plate was modeled using a viscoelastic double hardening model with combined shear-compression failure surface. The opening and the closing of the construction joints on the face plate were simulated using a discrete cracking model for concrete while the fill cushion layer-face plate interface was modeled using a modified Mohr-Coulomb law to represent the sliding-dilating behavior. In order to investigate the detrimental effects of stronger earthquakes on the structure, the nonlinear transient analysis presented in the work were conducted for increasing levels of ground motion as prescribed in the seismic risk study for the dam location.

There are some limitations to this study. First of all, the study is limited to a numerical prediction of the dam behavior, as laboratory and field monitoring data for

the investigated embankment are not available. Also, due to the incapability of a single constitutive hypothesis to simulate the mechanical behavior of an embankment dam under static and cyclic loading conditions, two different constitutive models and sets of parameters had to be used for the impounding and the transient earthquake analysis.

1.2 ÇOKAL DAM AND FINITE ELEMENT MODEL

The Çokal Dam is an 83-m-high CFRD with a crest length of 605 m that is constructed for irrigation and flood prevention in northwest of the Turkey at the Thracian Peninsula. The location of the dam site is less than 10 km from the North Anatolian Fault under the Marmara Sea. A typical cross-section of the dam is shown in Figure 1.1.a along with a selection of the materials that will be used at the site. The side slopes are 1H:1.4V, and the face plate is 50 cm thick. The reinforcement on the dam was assumed to correspond to 0.6% of the gross concrete area.

Two and three dimensional modeling and analysis were conducted for the Çokal Dam by the general purpose finite element software DIANA (TNO DIANA, 2008). A 2-D plane-strain model idealization (Figure 1.1.b) can be used due to the high aspect ratio of the dam (crest length/height=600 m/83 m=7.2). A total of 4600 six-node isoparametric plane-strain triangular elements with a three-point integration scheme were utilized to model the rockfill, and 54 three-node infinite shell elements, with each node having two in plane and one rotational degree of freedom, were utilized to show the face plate for the two 2D model. The infinite shell formulation, depending on the isoparametric degenerated solid approach given in DIANA (TNO DIANA, 2008), introduces two shell hypotheses, namely, the normal remain straight in the element and the stress that is perpendicular to the axis of the element is zero. Embedded reinforcements which do not have degrees of freedom of their own are

placed as an area in the face slab elements. A perfect bond between the reinforcement and the material is defined to system by the computation of the strains of the embedded reinforcement elements retrieved from the displacement field of the mother element. The connection between face plate elements and the rockfill is with line interface elements, based on quadratic interpolation, describing the relationship between the normal and shear tractions of interface. A nodal interface element was utilized at the bottom of the face plate to model separation from the foundation of the face plate at the plinth.

The embankment for the 3D model (Figure 1.1.c) was defined by 48000 10-node pyramid elements based on quadratic interpolation. A total of 4000 six-node iso-parametric curved shell elements were utilized to model the face plate. Vertical construction joints and the face plate-plinth base joints were simulated using 4000 line interfaces with 3+3 nodes, quadratically interpolated elements. Approximately 4000 plane interfaces in a 6+6 node configuration were used to simulate the interaction between the face plate and the rockfill. The 3D model had about 200000 degrees of freedom.

Finally, the Çokal Dam built on medium-hard rock with a Young's modulus that is about two orders of magnitude greater than the fill material, that's why; the foundation of the dam was not included in the models. The base was assumed to be a fixed support. Comparison of the 2 and 3D model results will be conducted for the results obtained at the middle of the dam at a representative cross-section as given in Figure 1.1.

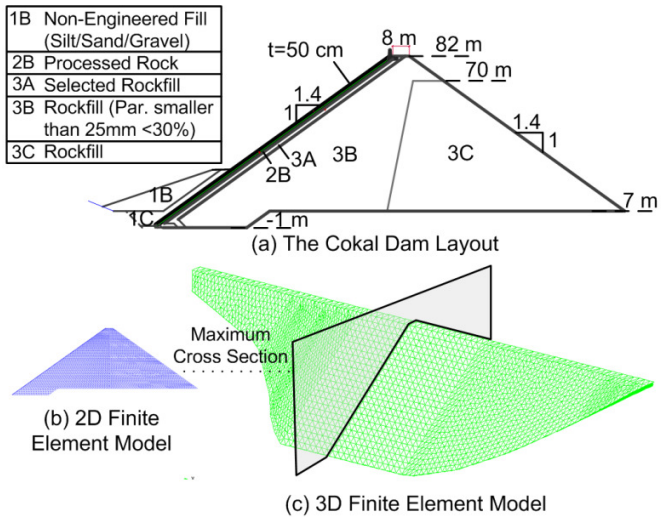

Figure 1.1 Çokal Dam Layout and Finite Element Models

For the 2D analyses (Figure 1.2), elements used are CL9PE and CT12E for the face plate and rockfill, respectively. CL9PE elements are numerically integrated infinite shell elements with second degree interpolation. For the interface between the rockfill and the plate, three-three node CL12I interface element was used. For the 3D analyses (Figure 1.2), CT30S and CTE30 elements were used for face plate and rockfill, respectively. CT30S elements are triangular curved shell elements with second degree interpolation. CT36I and CL18I elements (Figure 1.2) were utilized for interface between rockfill and face plate and between face plate and face plate, respectively. These elements contain multiple integration points.

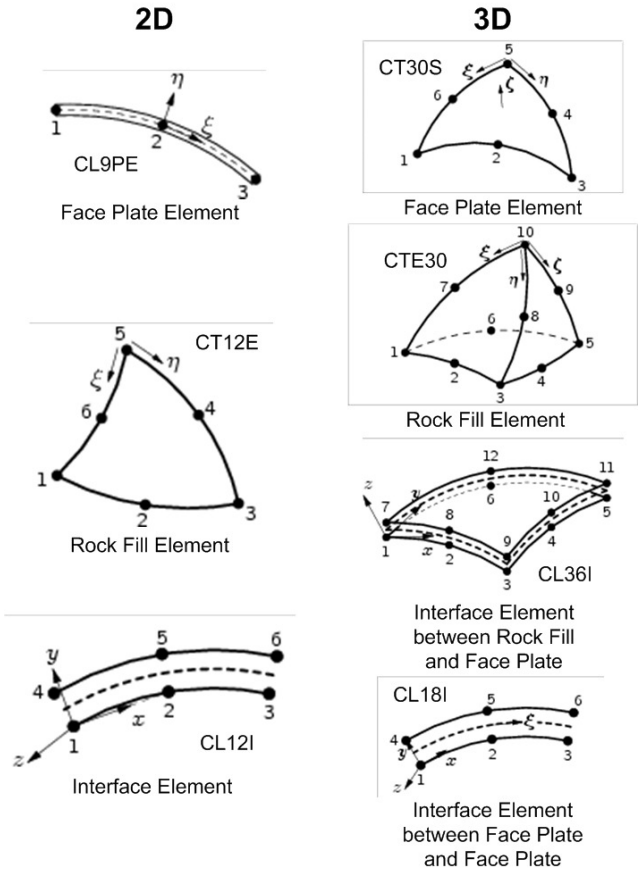

Figure 1.2 Finite Element Model Elements (TNO DIANA, 2008)

CHAPTER 2

CONCRETE FACED ROCKFILL DAMS, STRENGTH and MATERIAL CHARACTERISTICS

2.1 GENERAL

A definition of the rockfill dams, according to ASCE symposium on rockfill dams in 1960 is "a dam that relies on rock, either dumped in lifts or compacted in layers, as a major structural element." The definition implies dumped or compacted rock, with an impervious layer, namely; impervious membranes or earth cores to prevent the possible seepage on the dam body. Concrete is the most commonly used material for impervious membrane which is the material for this study. Other examples are asphalt for medium height dams, or steel and timber membranes. Generally, membranes are placed on the upstream face of the dams, however, in some cases; membranes are built inside the embankment of the dam (Singh and Varshney, 1995).

This chapter includes three main sections. First, the evolution, current trends and characteristics of CFRDs are presented. Next, the strength characteristics of the CFRDs are defined. The final part is comprised of the constitutive laws used for the modeling of CFRDs rockfill material.

2.2 EVOLUTION AND CHARACTERISTICS of CFRDs

2.2.1 CFRDs: From Past to Present

The evolution of the rockfill dams are considered under three main categories; early period (1850-1940), transition period (1940-1965) and modern period (1965-) by Cooke (1984). The early period of rockfill dams depended on California Gold Rush, as gold miners built rockfill dams to seek gold in California sierras. These dams had timber faces and steep slopes. The first known rockfill dam with concrete facing is Chatworth Park Dam (1895) that is in California. The Dix River Dam in Kentucky and Salts Springs Dam in California are the high dams recorded to be in the early period of the rockfill dams and their heights are 84 and 101 m, respectively. The operation of Salts Spring Dam lasted till 1931 in spite of its leakage problems. Rockfill dams' designs were promoted to earth core by 1940s; before rockfill dams were constructed with impervious membranes (Cooke, 1984).

The next generation of the rockfill dams is the transition period. For high rockfill dams (higher than 91 m), there were some limitations. One of them is to find suitable rock as a fill material. Until this period, the fill material was dumped rock which is considered to have high unconfined compressive strength. Another problem is the compressibility of the dumped rock since they were dumped in thick layers between 18 to 60 meters. This caused high settlement of the fill body and serious leakage problems in the dam during the impounding period of the reservoir. The 150m high New Exchequer Dam in California (1958) is the last dam built in this period. The dam was built 1.2-3.0 m lifts of partially compacted rockfill and 18 m lifts of dumped rockfill (Cooke, 1984).

The need for higher dams resulted in usage of new techniques to construct rockfill for the dam body. Dumped rock lost its popularity due to its side effects seen

in the transition period. A new era was started in rockfill dams using rock compacted with heavy machinery. The problems of unconfined strength and compressibility were overcome allowing higher dams with less leakage problems. This technique made possible the use of low quality rocks available throughout the dam sites with the invention of heavy machinery capable of large degree compaction. In contrast to the transition period, layers of rockfill are reduced to 3 m's. Ambuklao Dam is an example to this technique which is constructed in 1955. It had a layering of 0.6 m because of the availability and the use of low strength, low quality rock in the region (Cooke, 1984).

Thin layers of compacted rock, even if it was made from low quality rock, had a higher strength in compacted layers. This new development started the new period which can be called the modern period for CFRDs. With these new developments, CFRDs are alternative to earth core rockfill dams since availability of clay near dams' site is often lacking also increasing the cost of the dam. Many CFRDs are in construction all over the world and its popularity is increasing every day (Cooke, 1984).

2.2.2 Characteristics of CFRDs

2.2.2.1 Design of Dam Section

Design of CFRDs depends on essentially empirical data, and based on experience and judgment (Peck, 1980). Rockfill is located in the downstream, as the concrete wall behaves as an impermeable membrane to stop the release of water or the leakage from dam. Safety ratios are taken high for these dams against sliding and slope stability (Cooke, 1984). The higher portion of water load is carried via the

foundation of the dam body. 1.3H:1V to 1.5H:1V design slopes are commonly used since there wasn't failure due to slope stability of such dams in the past (Cooke, 1984).

2.2.2.2 Toe Slab

Hard, nonerodible rock which is groutable is the most desirable solution for the toe slab of foundation. Nevertheless, with proper engineering, any other materials could be acceptable to be the material of the toe slab, since the availability of the high quality; proper material may not be of a satisfactory amount. Several applications of for improvements of the site, namely; diaphragm wall, concrete backfilled backhoe trench or downstream filters or both, is for proper engineering of toe slab (Cooke, 1984). Again engineering judgment and the quality of the rock in the region have a role to determine the design of toe slab that is toe slab width. Near the top of the toe slab, one layer of reinforcement is used (Cooke and Sherard, 1987).

2.2.2.3 Face Slab

In CFRDs, durability and impermeability are the important considerations. Durability of the dam depends on its impermeability since a leakage problem causes the malfunctioning of the dam. The impermeability is satisfied by its concrete face. In practice, high strength concrete is not necessary; C20 concrete is thought as adequate for most of the designs (Cooke and Sherard, 1987).

The thickness of a CFRD face slab could be constant or linearly decreasing with height of the dam. As top of dam is considered zero datum point for calculation and the level that touches the ground is set as its height, a conventional equation

which is C+m*H is used to determine the thickness of the face slab, where C is a constant value, H is the height of the dam and m is a multiplier to determine the differentiation of the width of the face slab. For example, the thicknesses of the face slab for early dumped rockfill dams are calculated via the formulation that is 0.3 + 0.0067H (in m). In some CFRDs, m value is taken less than 0.002 (Cooke and Sherard, 1987).

In order to cope with the tensile stresses occurring on the face plate, reinforcement is placed in both directions of the slabs. The reinforcement ratios are selected around 0.4 or 0.5% or could be less. Reinforcement is prepared as a mesh in the face slab and placed on a single line on the centerline for changing width slabs or placed double layers for fixed width slabs. Double layer reinforcement also provides less spalling of the concrete. Reinforcement provides ductility, flexibility and higher deformation capacity to let the face slab accompany with rockfill by their interactions. This will allow small differential settlements without high bending stresses and provides bending resistance in both directions equally for face slab (Cooke and Sherard, 1987).

The concrete face is generally placed after the construction of the fill, except for some higher dams. The concrete slabs are placed vertically with horizontal construction joints from bottom to top. The range of the width of these strips change between 12-18m, 15 m is commonly used in practice.

2.2.2.4 Zoning in CFRDs

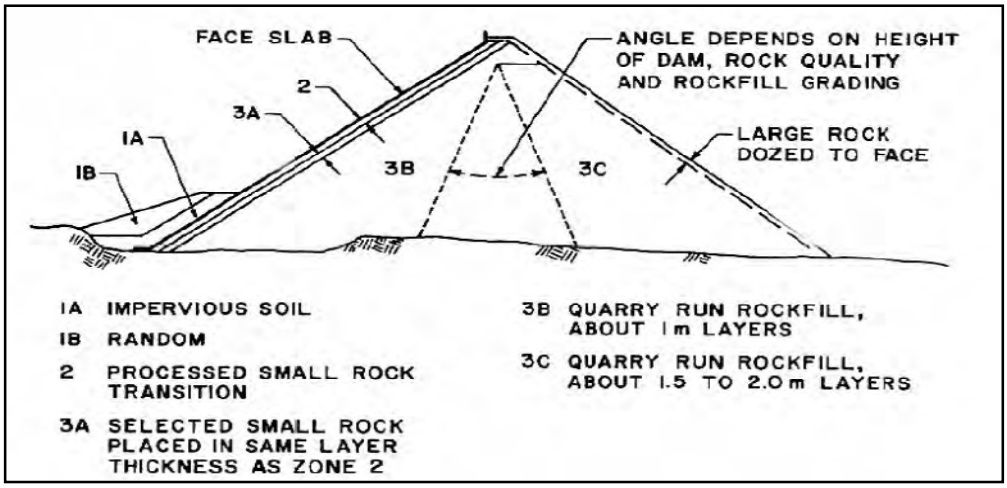

Figure 2.1 Zoning of CFRDs (Cooke and Sherard, 1987)

In Figure 2.1 above, a typical zoning of a CFRD is provided. Zone 1 has impervious soils that behave as blanket. Covering the perimeter joints and the slab in the lower elevations with an impervious soil is the goal of this zone. This will close cracks or joint openings. It is generally preferred in high dams but it is not a necessity for all CFRDs. Zone 1 can be placed from bottom to several meters above the original riverbed (Cooke and Sherard, 1987).

Zone 2 is composed of finer rock. The aim of using this zone is to provide a strong and uniform support for the slab. Rockfill materials that have particle sizes between 7.5 and 15 cm are used with 40% sand sizes and fines. Compaction is handled in 0.4-0.5 m layers using smooth drum vibratory rollers.

A semi-impervious barrier to prevent any leakage which can be produced through a crack in the concrete slab was provided by zone 2. To grant more workability and less permeability, more sand sized particles should be used in zone 2 (Cooke and Sherard, 1987). Nevertheless, this can cause a problem in rainy sites due to erosion.

Zone 3 is the main zone in a CFRD. This zone consists of three inner zones; Zone 3A, Zone 3B and Zone 3C. Zone 3A is a transition zone between Zone 2 and the rockfill. This layer is compacted in 0.4-0.5 m layers same as Zone 2. Compaction provides a limit to the size of the voids in Zone 3 A so as to make sure that the Zone 2 material not being washed into the larger voids with the main rockfill zones (Cooke and Sherard, 1987). Zone 3B is compacted in 1 m layers with 4-6 passes of a smooth drum vibratory roller. In order to control the slab displacements, the compressibility of Zone 3B should be as low as possible. The practices mentioned above yields a satisfactory performance (Cooke and Sherard, 1987).

Zone 3C has the least effect on the slab settlement and takes a lesser portion of the water load. This zone is compacted in 1-2 m layers with a couple of passes of smooth drum vibratory rollers. At the downstream face of the dam, large rock particles are usually placed (Cooke and Sherard, 1987).

2.2.3 Grading and Materials for the Rockfill Body

There are no clear rules in order to specify the rock used for the fill material in a range. However, there are some expectations from the fill material. The rock that is used for fill of the dam should be durable and resistant to weathering. To satisfy these requirements, hardened rocks, such as; igneous or metamorphic rocks could be suitable to use. For example, granites, diorites, basalts, dense sandstones and limestone could be used as the fill material of the rockfill dams.

The unconfined compressive strength of the rockfill used in CFRDs has a range between 10 MPa (lowest) to more than 245 MPa (highest). Generally this range in applications is between 50-150 MPa. Most of the time, 30 MPa hard rocks are considered to be suitable for CFRDs. Higher strength materials do not provide extra advantage to structure since 30-40 MPa unconfined compressive strength rocks cannot provide more compressibility than 30 MPa rocks when the dam is completed. Besides, the usage of rock with a lower compressive strength has certain advantages; it is less costly to blast and causes less damage to rubber-tired equipment (Cooke and Sherard, 1987).

Cooke (1984) suggests that the behavior of the rock after wetting is one of the most important issues for selecting the type of the rock. If a blasted rockfill is strong enough to support construction trucks and a 10 tons vibratory roller after wetting, then it is assumed to be suitable to use for compacted rockfill dams. If the rock breaks apart and cannot stay draining after compaction, zones of hard, pervious rockfill should be provided for internal drainage. Increasing density of the rockfill could increase the sustainability and durability against wetting of the material, thin layers of weak rock (layers about 2 ft) could increase the density of the rockfill since hard rock has lower density and providing thin layers of weak rock provides interlocking of the fill (Cooke, 1984).

According to Cooke and Sherard (1987), a stable construction surface under the traffic loads caused by heavy trucks shows that the wheel loads are being carried by skeleton of the rockfill, on the other hand, an unstable construction surface means that loads are carried by the finer particles. If an unstable surface exists, the resulting embankment may not have the properties suggested for a pervious rockfill body.

2.2.4 Sluicing

Sluicing is to add water to the rockfill during its construction period. The purpose of adding water is to soak the material and to soften the fine particles. The compressive strength of the rockfill is decreased and finally, embankment presents lower settlements after the construction. In case of a very low water absorption capacity of the rock that is used, the improvement in compressibility could be very small and be taken as negligible. This situation is for dams of moderate height and for Zone 3C.

The amount of water spent in sluicing should be between 10-20% of the rockfill embankment volume. The addition of water has less effect on the behavior of the dam for most hard rocks and CFRDs of low to moderate heights. Water should be added seasonally for the upstream shell (Zone 3B) for high dams and for rock having significantly lower unconfined compressive strength while they are tested in wetted condition. For the case of rockfill that have high contents of earth and sand-sized particles, water should nearly always be used. Water softens the fines of dirty rocks so that larger rock particles can be in contact with each other due to the effect of the vibrating roller (Cooke and Sherard, 1987).

2.3 STRENGTH CHARACTERISTICS for CFRDs

2.3.1 Shear Strength Characteristics for Rockfill

Shear strength is essential to understand the behaviors of the CFRDs. However, the determination of this characteristic of rockfill is a challenging issue for civil engineers. Conventional laboratory triaxial tests are not suitable since the

rockfill materials have particles up to 1200 mm particle sizes. It is not sensible to obtain test apparatus for these large materials because this would not be economic. However, tests to establish the strength properties of rockfill should be conducted: for this reason, some special methods are used to reduce the size of the specimen to overcome this problem.

Gradation of rockfill materials also leads to different mechanical properties for the fill. The study published by Varadarajan et al. in 2003 presents triaxial test results on two different rockfill materials obtained from different sites, Ranjit Sagar Dam and Purulia Dam Sites in India. According to the impact, crushing and LA abrasion tests, the Ranjit Sagar rockfill particles were stronger than the other rockfill material. Triaxial tests were conducted in drained condition with the specimens having 25, 50 and 80 mm max particle sizes. For the Ranjit Sagar material, testing was conducted at 0.35, 0.70, 1.1 and 1.4 MPa confining stresses, whereas the Purulia rockfill material was tested at 0.3, 0.6, 0.9 and 1.2 MPa confining. The results of the triaxial tests are presented in Figure 2.2.

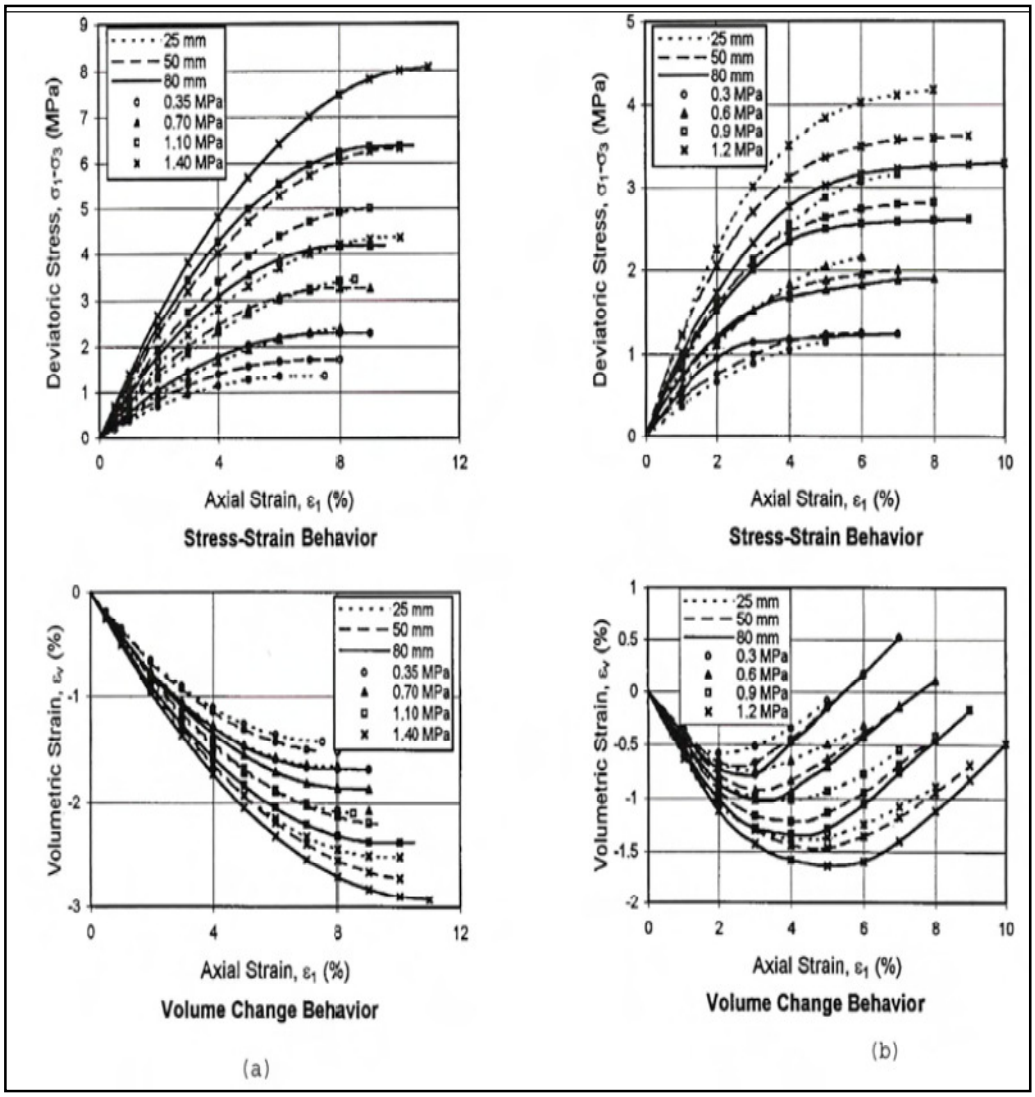

Figure 2.2 Triaxial test results of two rockfill specimens (Ranjit Sagar Dam specimens, Purulia Dam specimens, Varadarajan et al., 2003)

The gradation of the fill effects the material properties differently for Ranjit Sagar and Purulia fills. While an increase in maximum particle size leads to a more rigid fill failing at a higher deviatoric stress for the Ranjit Sagar fill, for the Purulia Dam the effect is reversed. The graphs shown above prove the necessity of triaxial tests to obtain the mechanical characteristics of the rockfill of CFRDs.

2.5 DYNAMIC RESPONSE of CFRDs

CFRDs with compacted rockfill are generally thought to display a high resistance to seismic loading. As long as the rockfill body is kept dry by their impervious layer, they can show higher resistance (Cooke, 1984). The 84 m high Cogoti CFRD is shown as an example of a compacted rockfill dam withstanding a moderate earthquake in its region that kept its serviceability. The results showed that rockfill in the crest area loosened and several meters of settlement, however, below the water level, face slab showed no movement (Cooke, 1984).

The softening of the rockfill or a loss of strength occurs in soils under earthquake motions. Reduction of the stiffness can be observed generally in saturated loose to medium cohesionless soils. Extreme forms of this behavior are generally called soil liquefaction or cyclic mobility. For saturated cohesionless soil under cyclic loading, increase in the pore pressure due to rapid loading leads to decrease in the effective stress, causing liquefaction (Özkan, 1998).

Another important issue is the effect of the face plate on the response of the CFRDs. Kong and Liu (2002) analyzed a CFRD under dynamic loading with the discontinuous deformation analysis (DDA). The slab was shown to lose its support under strong earthquake by the failing of the soil mass that includes loosening, sliding and subsiding, leading to fracture occurring in the upper portion of the facing slab.

Thus, improving downstream slope stability provides the stability of concrete-faced rockfill dams (Kong and Liu, 2002).

Another issue is the dimension of the analysis. 2D and 3D analysis have different outcomes due to their natures. Dam and side valley interaction appears to be the strongest influence on the body of the dam (Boulanger et. al., 1995). 3D analyses comply the actual fundamental period of the earthquake ground motions at the finite element analysis of Cogswell Dam. The study of Feng et al. (2010) consists of the 3D response of the CFRDs. The case study is the Miaojiaba CFRD. The deformation between the toe slab and the bottom edge of the face slab is determined to be larger than the deformation between the face slab and the bedrock (Feng et al., 2010).

In conclusion, the dynamic response of the CFRDs is influenced by many factors. These factors are material properties, liquefaction or cyclic mobility, homogeneity of the section of the CFRD and the valley effects, along with other site specific concerns. What one should consider is that, erroneously, for all fill dams with concrete facing, the nomination CFRD is commonly used. Gravel and sandfill dams are categorized by designers as CFRDs and treated similarly, which indeed possess very different dynamic properties and perhaps the risk of cyclic mobility. The nonlinearity determined by the combination of the factors given above defined the behavior of the CFRDs in seismic excitation.

CHAPTER 3

MATERIAL MODEL

In this chapter, constitutive models that are used to in the simulations are described. Three main parts of the model, namely; reinforced concrete, rockfill and the interface between the fill and the concrete plate are presented in this chapter. Due to the variety of the analysis, different models were utilized to define model that will be covered here. (Compressive stresses are expressed as negative and tensile stresses are expressed as positive.)

3.1 REINFORCED CONCRETE

The constitutive model utilized for concrete is the total strain fixed-crack model (Feenstra et al. 1998). Total strain crack models evaluate the stresses in the crack directions of the plate. Fixed crack model evaluates the stress-strain relationships in a coordinate system which is fixed upon cracking. The strain vector $\boldsymbol{\varepsilon}_{\mathbf{xyz}}(t_i)$ is renewed by the strain increment $\boldsymbol{\Delta\varepsilon}_{\mathbf{xyz}}(t_i + \Delta t_i)$ in the element coordinate system:

$$\boldsymbol{\varepsilon}_{\mathbf{xyz}}(t_i + \Delta t_i) = \boldsymbol{\varepsilon}_{\mathbf{xyz}}(t_i) + \boldsymbol{\Delta\varepsilon}_{\mathbf{xyz}}(t_i + \Delta t_i) \tag{3.1}$$

The strain $\boldsymbol{\varepsilon}_{\mathbf{xyz}}(t_i + \Delta t_i)$ is turned into the strain vector in the crack direction $\boldsymbol{\varepsilon}_{nst}(t_i + \Delta t_i) = \mathbf{T}\boldsymbol{\varepsilon}_{\mathbf{xyz}}(t_i + \Delta t_i)$ with the transformation matrix $\mathbf{T}$. The constitutive model is then used within the crack coordinate system which is given by

$$\boldsymbol{\sigma}_{\mathbf{nst}}(t_i + \Delta t_i) = \boldsymbol{\sigma}(\boldsymbol{\varepsilon}_{\mathbf{nst}}(t_i + \Delta t_i)) \tag{3.2}$$

The updated stress vector in the element coordinate system is given by the transformation:

$$\boldsymbol{\sigma}_{\mathbf{xyz}}(t_i + \Delta t_i) = \mathbf{T}^T \boldsymbol{\sigma}_{\mathbf{nst}}(\boldsymbol{\varepsilon}_{\mathbf{nst}}(t_i + \Delta t_i)) \tag{3.3}$$

The zone of the compression of the concrete is defined by a parabolic response, with f_c defining the peak strength (Figure 3.1). The crushing behavior and ultimate strain are determined by the compressive fracture energy G_c. This makes the model to be objective and mesh-independent (Arıcı 2011). A linear softening function beyond the tensile strength f_t defines the tensile behavior of the concrete model. The ultimate tensile strain is defined by the tensile fracture energy G_f^I. The utilized tensile-compressive constitutive relationships can be seen in Figure 3.1.a. where *h* represents the effective element size. Figure3.1.b represents a typical strain hardening diagram that was chosen for the embedded reinforcement with the stress-strain diagrams, where f_y and ε_y shows the yield strength and strain, respectively.

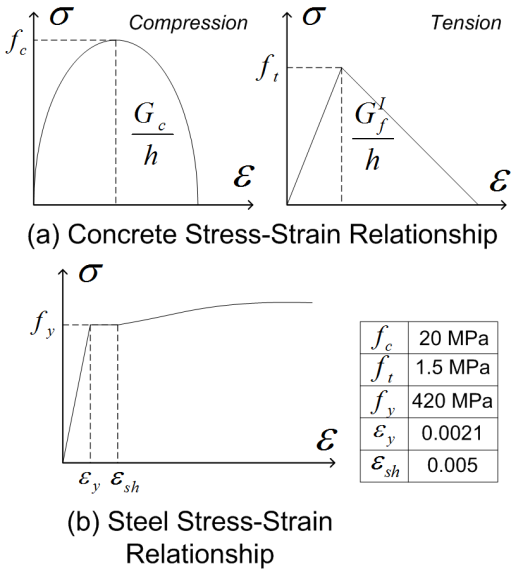

Figure 3.1 Constitutive Relations for a Reinforced Concrete Face Plate (Arıcı, 2011)

Crack widths on the face plate were estimated using the empirically well-established Gergely-Lutz expression (1968), which is generally used in reinforced concrete design (ACI, 2004), relating the maximum crack width $w_{\max}$ to three variables: the reinforcement steel strain at the crack (ε_{scr}), the concrete cover over the reinforcement d_c and the area of concrete around each bar A :

$$w_{\max} = 2.2\beta_{GL}\varepsilon_{scr}\sqrt[3]{d_c A} \tag{3.4}$$

where β_{GL} is a factor that accounts for the strain gradient within the member.

3.2 ROCKFILL CONSTITUTIVE MODEL

3.2.1 Rockfill Constitutive Model in Static Loading

Triaxial experiments (Varadarajan et al., 2003) conducted on rockfill specimens show that the stress-strain behavior of rockfill material is nonlinear, inelastic and stress-dependent, moreover, an increase in the confining pressure increases the values of the peak deviatoric stress, axial strain and volumetric strain at failure and an increase in the size of the particles increases the volumetric strain at the same confining pressure. The strength envelope of rockfill specimens is curved which means that an increase in the confining stress causes a decaying increase in the deviatoric stress for higher confining stress levels. This shows a decrease of the friction angle accompanied with the confining pressure. A modified Mohr-Coulomb formulation (TNO Diana, 2008), as conducted in tests of Groen (1995), was utilized in this study. The hardening of the rockfill with increasing shear stress, the volumetric deformations and the dependency of the mechanical properties on the confinement stress are modeled by the Mohr-Coulomb formulation. The nonlinear elasticity combined with hardening shear yield surface and a circular-shaped compression cap is used in this constitutive relationship (Arıcı, 2011). The compression modulus K_t is assumed as some power $(1-m)$ of the mean effective stress level $p' = 1/3\,(\sigma'_{xx} + \sigma'_{yy} + \sigma'_{zz})$ and the reference compression modulus K_{ref} as provided in Eq. 3.5:

$$K_t = K_{ref}\left(\frac{p' + p'_t}{p_a}\right)^{1-m} \tag{3.5}$$

$$\left(\frac{p' + p_t'}{p_{ref}'}\right)^{m-1} dp' = K_{ref} d\varepsilon_v^e \tag{3.6}$$

where p_a and p_t' show the atmospheric pressure and a compression offset value utilized to define the model performance for tension, respectively. The tangent shear modulus G_t can be defined by assuming a constant Poisson ratio (υ) (Eq. 3.7). Nonlinear elasticity is defined in terms of the volumetric components.

$$G_t = \frac{3}{2} K_t \frac{1-2\upsilon}{1+\upsilon} \tag{3.7}$$

A double hardening model in which the shear and compressive failures are uncoupled is the yield function for this model. In $p' - q'$ space, where q' defines the deviatoric stress, the functions (f_1) and (f_2) defining the shear and compression failure surfaces (Figure 3.a) can be expressed as:

$$f_1 = \frac{q'}{R_1(\theta)} - \frac{6\sin\phi}{3-\sin\phi}(p' + \Delta p') = 0 \tag{3.8}$$

$$f_2 = (p' + \Delta p')^2 + \frac{2}{9} q'^2 - p_c^2 = 0 \tag{3.9}$$

where ϕ is the friction angle, $\Delta p'$ is the pressure shift for the shear yield surface, p_c is the preconsolidation pressure, and $R_1(\theta)$ is a function of Lode's angle θ . The

function $R_1(\theta)$, given in Eq. 3.10, accounts for the difference in the triaxial strength for compression and extension by making use of Lode's Angle θ and the factor β_1.

$$R_1(\theta) = \left(\frac{1 - \beta_1 \sin 3\theta}{1 - \beta_1} \right)^{-0.229} \tag{3.10}$$

$$\beta_1 = \left(\frac{3 + \sin\phi}{3 - \sin\phi} \right)^{\frac{-1}{-0.229}} - 1 \Bigg/ \left(\frac{3 + \sin\phi}{3 - \sin\phi} \right)^{\frac{-1}{-0.229}} + 1 \tag{3.11}$$

The direction of the inelastic strain rate is set by the plastic potential surfaces g_1 and g_2 given in Eqs. 3.12, 3.13, where ϑ shows the angle of dilatancy.

$$g_1 = q' - \frac{6 \sin\vartheta}{3 - \sin\vartheta} (p' + \Delta p') \tag{3.12}$$

$$g_2 = (p' + \Delta p')^2 + \frac{2}{9} q'^2 - p_c^2 \tag{3.13}$$

The progress of the shear yield surface is determined by a multi-linear differentiation of the sine of the friction angle ($\sin\phi = \sin\phi(\kappa_1)$) with respect to an internal model variable κ_1 (Figure 3.2b), while the progress of the compression cap is determined by changes in the preconsolidation pressure p_c with respect to an internal variable κ_2.

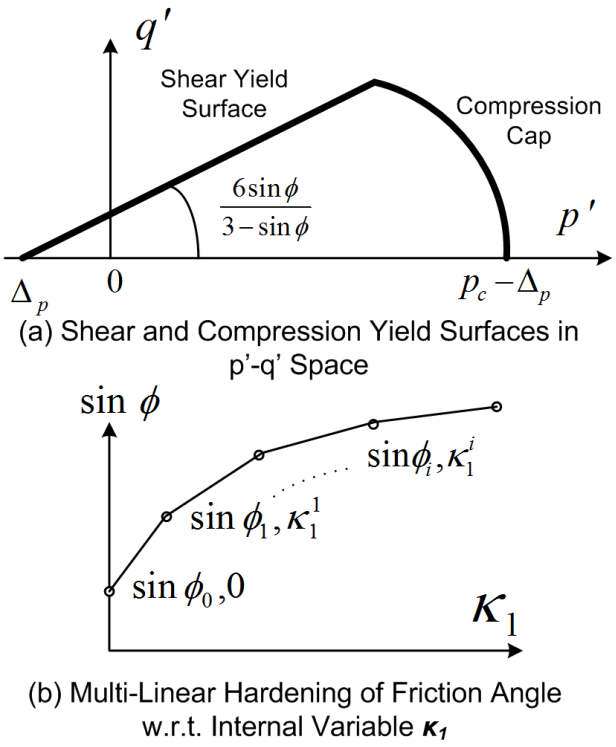

Figure 3.2 Rockfill Constitutive Model (Arıcı, 2011)

According to Rowe's stress dilatancy theory, the dilatancy angle ϑ is a function of the friction angle, where ϕ_{cv} is a constant value that can be exposed as the friction angle at constant volume.

$$\sin\vartheta = \frac{\sin\phi - \sin\phi_{cv}}{1 - \sin\phi\sin\phi_{cv}} \tag{3.14}$$

The evolution of the friction angle $\sin\phi = \sin\phi(\kappa_1)$ is used to model the hardening behavior which is done to define the shear failure surface. Figure 3.2.b represents multi-linear variation of the friction angle with respect to the internal variable κ_1. The formerly defined multi-linear variation of this formulation can represent hardening and softening. However, softening terms were not necessary to utilize in this study (Arıcı, 2011). κ_1 is updated by the equivalent plastic deviatoric strain increment $\Delta\boldsymbol{\gamma}^p$ and a diagonal factor matrix $\mathbf{R}$ (Eqs. 3.15, 3.16) for this model. A detailed description of the model is provided in Arıcı (2011).

$$\Delta\kappa_1 = \sqrt{\left(\frac{2}{3}\right)\left(\Delta\boldsymbol{\gamma}^p\right)^T \mathbf{R}\left(\Delta\boldsymbol{\gamma}^p\right)} \tag{3.15}$$

$$\mathbf{R} = \begin{bmatrix} 1 & 0 & 0 & 0 & 0 & 0 \\ 0 & 1 & 0 & 0 & 0 & 0 \\ 0 & 0 & 1 & 0 & 0 & 0 \\ 0 & 0 & 0 & 1/2 & 0 & 0 \\ 0 & 0 & 0 & 0 & 1/2 & 0 \\ 0 & 0 & 0 & 0 & 0 & 1/2 \end{bmatrix} \tag{3.16}$$

Detailed test results from Varadarajan et al. (2003) were assumed and used as the material properties in this study given the lack of detailed triaxial testing of Çokal rockfill material. The mechanical properties of rockfill for the static analysis results on the constitutive model was calibrated to triaxial tests that were conducted at three levels of confining stress (i.e., 0.35, 0.7 and 1.1 MPa) for different rockfill gradations,

namely; D25, D50 and D80. A comparison of the model predictionss and the triaxial test results for deviatoric stress and volumetric strain-axial strain are provided in Figure 3.3. Hardening of the shear yield surface is established by the multi-linear variation of the sine of the friction angle in this model. Hardening of the compression cap was not tried to calibrated, where the stress levels were below the stress state at which the cap yield surface is reached. The parameters for the constitutive model for D80 gradation are presented in Table 3.1.

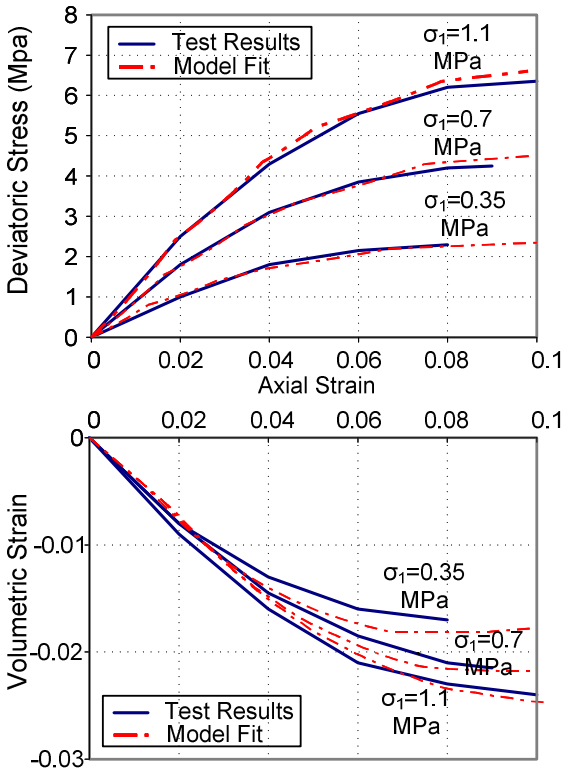

Figure 3.3 Comparison of Triaxial Test Results (Varadarajan et al., 2003) vs. Model Predictions (Arıcı, 2011)

Table 3.1 Model Parameters for the Rockfill (D80 Gradation) (Arıcı, 2011)

Parameter	D80
Common Parameters	$p_t' = 0.2MPa$ $\Delta p' = 0.02MPa$ $p_c = 1.5MPa$ m=0.20 υ=0.34
ϕ_{cv}	0.75
K_{ref}	20.0 MPa
$\sin\phi(\kappa_1^i)$	0.20(0.000) / 0.30(0.001) / 0.40(0.002) / 0.50(0.004) / 0.55(0.006) / 0.60(0.008) / 0.61(0.009) / 0.63(0.010) / 0.65(0.014) / 0.68(0.018) / 0.70(0.025) / 0.72(0.030) / 0.74(0.050) / 0.78(0.400)

3.2.2 Rockfill Constitutive Model in Dynamic Loading

The modified Ramberg-Osgood formulation (TNO DIANA, 2008) is defined to simulate the behavior of fill during cyclic loading. The stiffness degradation and the hysteretic damping of the rockfill material under cyclic strain are described in this model by Eqs. 3.25, 3.26. The parameters α and β that define the dynamic backbone function for this formulation are defined utilizing the reference shear strain (γ_r) and the maximum damping value ($\xi_{\max}$).

$$\gamma_{xy} = \frac{\sigma_{xy}}{G}\left(1 + \alpha\left|\tau_{xy}\right|^{\beta}\right) \tag{3.25}$$

$$\alpha = \left(\frac{2}{\gamma_r G}\right)^{\beta} \;\&\; \beta = \frac{2\pi\xi_{\max}}{2 - \pi\xi_{\max}} \tag{3.26}$$

$G = G_{ref}\left(p'/p_a\right)^{0.5}$ was assumed as the tangent shear modulus in the above formulation, defined by the current mean effective stress p', the atmospheric pressure p_a and the reference shear modulus. The unloading and reloading behavior is described by Masing's rules (Kramer, 1996).

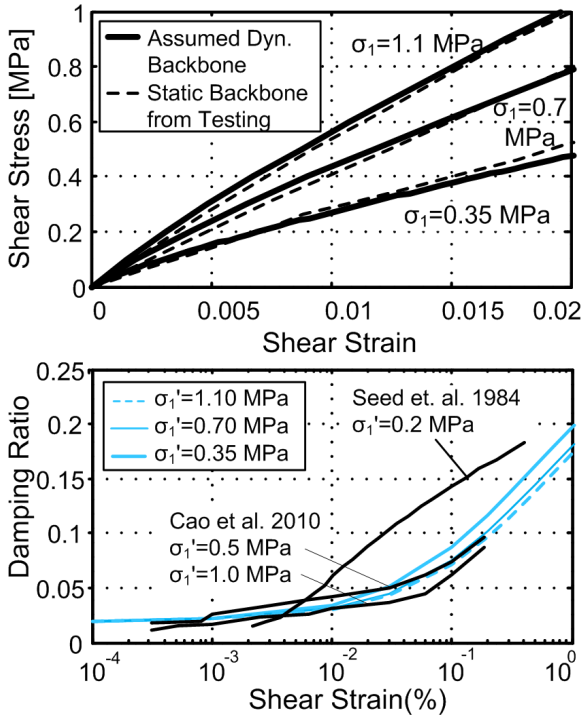

Figure 3.4 Performance of the Dynamic Model (Arıcı, 2011)

The reference shear strain in Eq. 3.25 as a function of the mean stress p' ($\gamma_r = a\exp(bp')$) at a given location within the fill, enabling to define the confining stress dependency of the damping ratio and stiffness degradation (Seed et al., 1984). The parameters $a = 0.0038$ and $b = 0.0040$ were obtained by calibrating the backbone curves at three confinement levels to tests results in (Varadarajan et al., 2003), as given in Figure 3.4. The shear strain vs. damping ratio curves obtained from the model fit well with the test results for Changheba Dam (Cao et al., 2010) rockfill; however these results are somehow lower than the curves provided for Oroville Dam material in (Seed et al., 1984). A 2% viscous damping was implemented to the model

by utilizing Rayleigh damping to get the low damping which is provided by the Ramberg-Osgood formulation at very small shear strains. Different values of γ_r were calculated for each plane-strain element within the embankment depended on the mean effective stress p' of an element at the end of impoundment (EoI) stage.

3.3 INTERFACE MODELING

Experimental data defining the interface behaviors of CFRDs are rather limited (Zhang et al., 2009, Uesugi et al., 1990). Shear tests of monotonic and cyclic on the interface were implemented in models (Uesugi et al., 1990). According to models (Uesugi et al., 1990), failure of the interface is a combination of contact and filler failure. The tests conducted for interface between face slab and gravel cushion layer showed a friction-dominated response with volumetric dilation (Zhang et al., 2009). Residual friction coefficients between 0.6 and 0.8 were obtained. According to the results of these studies, the interface between the slab and the cushion layer was considered to be determined by frictional behavior represented using a simple Mohr-Coulomb plasticity model (TNO DIANA, 2008, Vermeer and De Borst, 1984). The Coulomb friction model uses the following yield (f_I) and plastic potential (g_I) surfaces provided in terms of the normal traction t_n and the tangential traction t_t.

$$f_I = \sqrt{t_t^2} + t_n \tan \phi_I - c_I = 0 \tag{3.27}$$

$$g_I = \sqrt{t_t^2} + t_n \tan \vartheta_I \tag{3.28}$$

where $\tan\phi_I$ and c_I are the friction coefficient and the cohesion, respectively. $Tan\,\vartheta_I$ shows the tangent of the angle of dilatancy. The rate of plastic displacement $\Delta\dot{u}^p$ is governed by:

$$\Delta\dot{u}^p = \dot{\lambda}\frac{\partial g}{\partial t} \tag{3.29}$$

where $\dot{\lambda}$ is a multiplier. The tangent stiffness matrix is nonsymmetrical in case the friction angle is not equal to the dilatancy angle ($\phi_I \neq \vartheta_I$). The interface element was calibrated according to the test results represented in (Zhang et al., 2009) for a concrete-gravel layer contact, as shown in Figure 3.6. The agreement is reasonable, however, at later stages, dilation is overestimated.

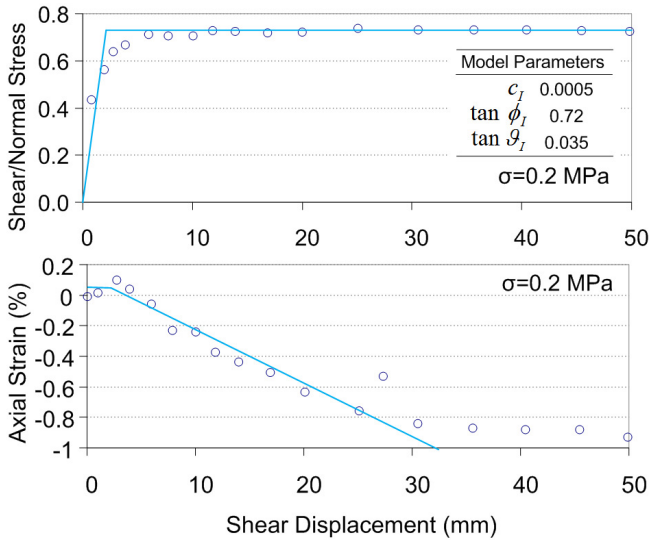

Figure 3.5 Comparison of Shear Friction Tests (Zhang et al., 2009) vs. Model Predictions (Arıcı, 2011)

3.4 FACE SLAB-PLINTH INTERFACE

A discrete cracking model (TNO DIANA, 2008) was utilized for the constitutive relation in the interface between the face slab and the plinth. When the tensile strength, (f_t) of the element is reached, a brittle failure was assumed accompanied with the full reduction of element strength. Once the cracking occurs, the shear stiffness of the interface was also reduced to zero. A similar model was utilized to simulate the behavior of the interfaces at the construction joints between the strips of the face plate.

CHAPTER 4

ANALYSIS OF CFRD's

4.1 STATIC ANALYSIS FOR IMPOUNDING

4.1.1 Analysis Technique:

CFRD deformation during impounding and earthquake loading depends on intact particle strength, rockfill gradation, mineralogy, foundation conditions as well as construction technique and loading. After the fill is built by sequential placement and compaction of thin layers of processed rock, the face plate is cast-in place on the fill. The settlement of the rockfill during the construction and the impounding stage is a loading condition on the fill; the transfer of the loading is controlled by the face-plate-cushion layer interface with stick-slide behavior. Modeling of the loading stages of the plate is important to realistically predict the behavior of the face plate as the transfer is dependent on three non-linear acting components, i.e. the face plate concrete, the interface filler material and the rockfill. To represent a proper loading sequence, the rockfill is completed in 27 stages in 3m increments for the 2D model, after which, the concrete plate is created on the top of the rockfill connected to it with interface elements. The impounding process is modeled with water rising to the maximum water level (MWL) in 27 steps. The sequence of modeling for this case is presented in Figure 4.1.a. For the 3D model, the fill is created in a single step, followed by the birth of the face plate model on top of the fill, later to be loaded

incrementally with rising reservoir similar to the 2D model. As the face plate construction happened independently of the fill construction, (the face plate rests on the deformed configuration of the plate), the stress state on the plate in both cases were obtained very similar.

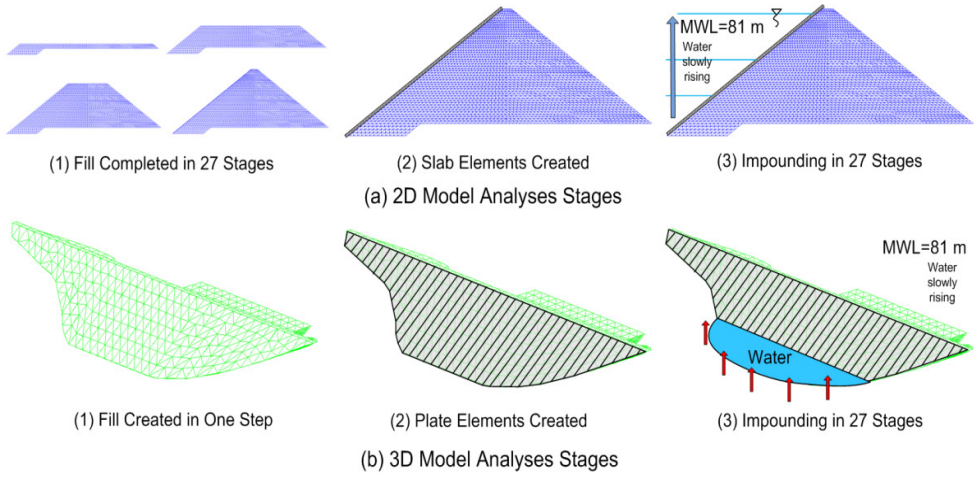

Figure 4.1 2D and 3D Analysis Schemes Representing Loading Stages

4.1.2 Comparison of 2D-3D Models

During the impounding of the reservoir, the displacements of a CFRD are not significantly different for 2 and 3D cases. The impounding of the reservoir changes the state of stress relatively significant only near the upstream face of the dam. The state of stress after impounding for the 2D and 3D models are compared in Figure 4.2.

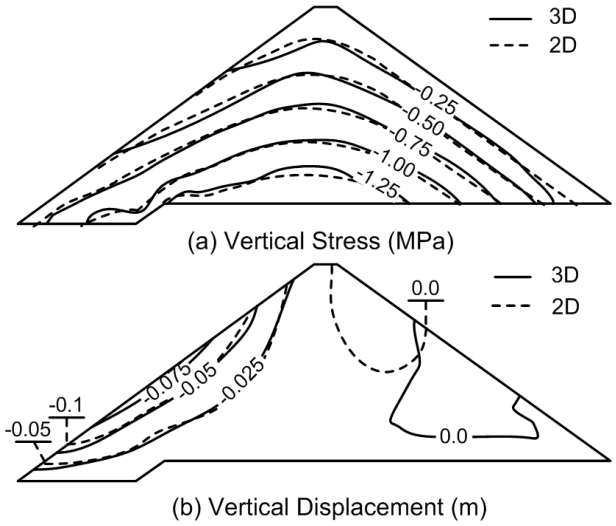

Figure 4.2 The State of Stress and Settlement after the Impounding

As seen in Figure 4.2.a, vertical stresses on the fill in the maximum cross-section at MWL were very similar. The displacements shown in Figure 4.2. also were not significantly different for 2D and 3D models. However, the effect of the valley sides on the body reduces the results of the displacements for the 3D model.

The change in the state of stress on the face plate at the maximum cross section for different water levels are provided in Figure 4.3 for 2 and 3D models. The form of stress levels on the face plate for the 2 and 3D models agree well.

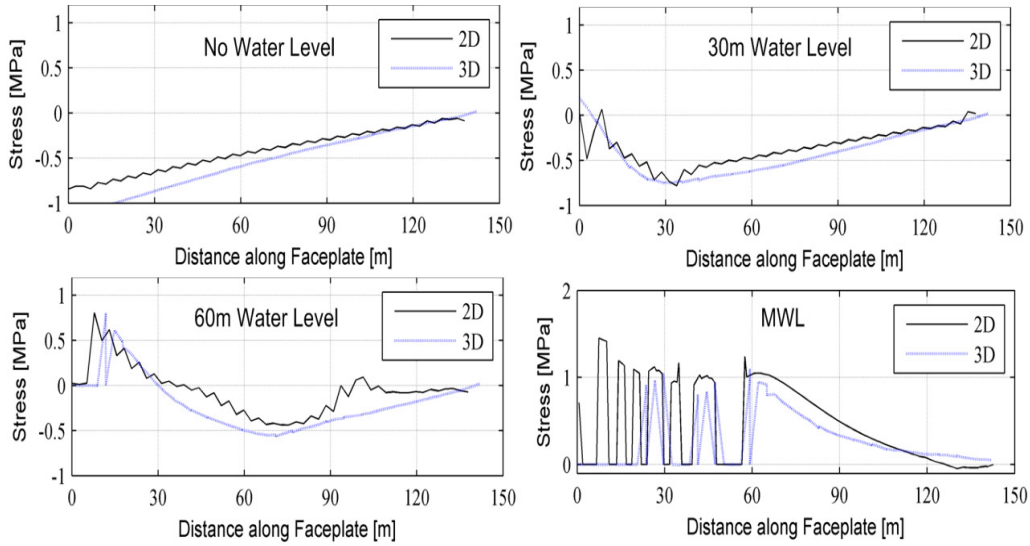

Figure 4.3 State of Stress on the Face Plate during the Filling of the Reservoir

Figure 4.3 shows that face plate was under compression and increasing towards the plinth when the reservoir was empty. However, during impounding, tensile stresses are generated slowly on the face plate. At MWL, from base to 60 m level, cracking is observed with zero stress levels. Moreover, at MWL, face plate is completely under tensile stress.

The formation of cracking on the face plate for the 2 and 3D models agree well. At MWL, cracking spreads 55-60 m from the plinth level towards the crest for both models (Figure 4.4). The 2D model represents the cracking behavior better due to the mesh density: the residual stresses between the cracked elements of the face plate were obtained more clearly. The widths of the cracks on the face plate were obtained similarly for both models as well as given in Figure 4.4. The maximum crack width obtained for both models was around 0.5 mm.

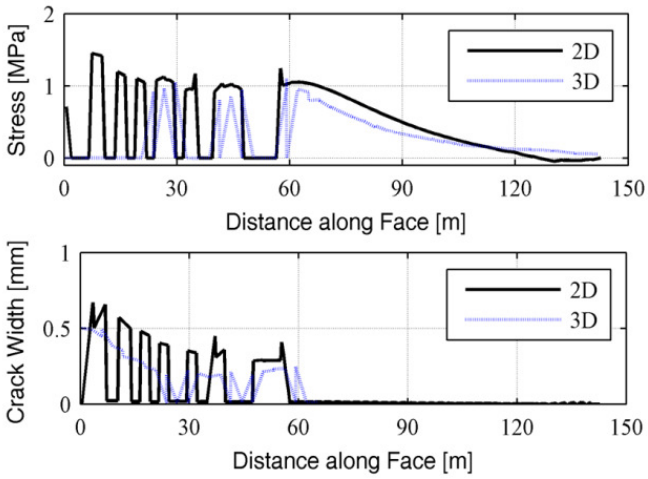

Figure 4.4 The State of Cracking on the Face Plate at MWL

4.1.3 3D Effects

The state of stress on the face plate near the valley ends cannot be obtained in a 2D analysis. The state of in-plane stress on the plate in the horizontal and vertical directions, as obtained from the 3D analyses of the Çokal Dam, is shown in Figure 4.5.

2D analysis is limited in the sense that it cannot determine the state of stress near the valley boundaries on the face plate, the behavior of the vertical construction joints on the plate the formation of the tensile and shear cracking on the face plate due to stresses parallel to the dam axis. In Figure 4.5.g, cracking of the plate is marked as gray resulting in discontinuities on stresses of faceplate. At MWL, faceplate is significantly cracked.

After the construction stage, the stress in the horizontal direction that is parallel to the dam axis is very small on the faceplate (Figure 4.5). Submerged areas

of the faceplate are the places where the tensile stresses in horizontal direction were started to be observed during impounding. At MWL, the face plate is under the largest compressive stress at the center. The edges of the plate are under tensile stresses. Tensile stresses are also obtained in the crest of the dam.

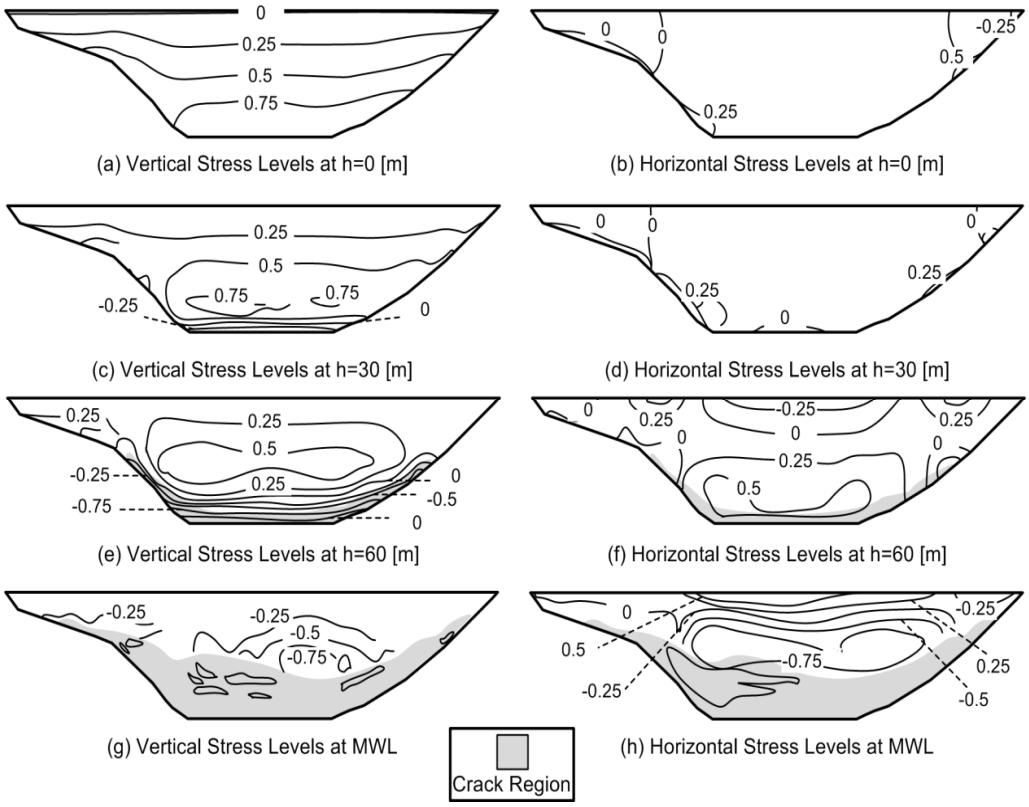

Figure 4.5 The State of Stress on the Face Plate (in MPa)

The detailed sketch of the cracking on the face plate is provided in Figure 4.6 Horizontal cracks developing parallel to the dam axis (opening in the vertical direction) are the main cracks observed on the at MWL. Vertical cracking are only observed, with very small crack widths (less than 0.1 mm), at the edges of the faceplate boundaries near the valley sides as shown in Figure 4.6.

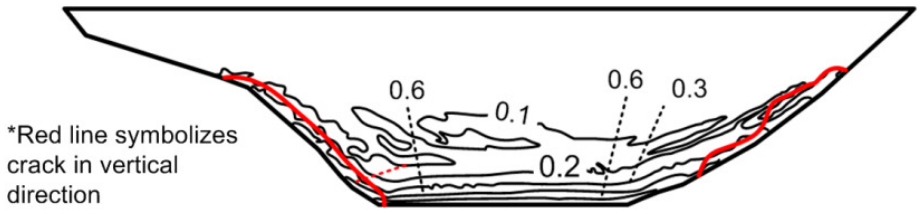

Figure 4.6 Contours of Crack Width at the Maximum Reservoir Level (in mm)

The tensile strength of the cold joints in the Çokal Dam at the vertical interfaces was not exceeded. The determination of the vertical joints that will open during impounding is an important issue for designers, as these joints are detailed with water stoppers in contrast to compression joints. In Figure 4.7, the opening of the vertical joints that is normal to the interface plate is sketched. The maximum value obtained from the 3D analysis is about 0.1 cm which can be easily tolerated with the material provided for the vertical joints. The opening of the joint near the plinth base is presented in Figure 4.8. The maximum separation between the plinth base and the face plate is 0.5 cm from the 3D analysis, however, this was obtained 0.8 cm from 2D analysis. 75% of the bottom surface of the face plate is almost uniformly separated from the plinth base as shown in Figure 4.8. The separation

between the plinth base and base of the face plate disappears near the top of the valley sides for the dam.

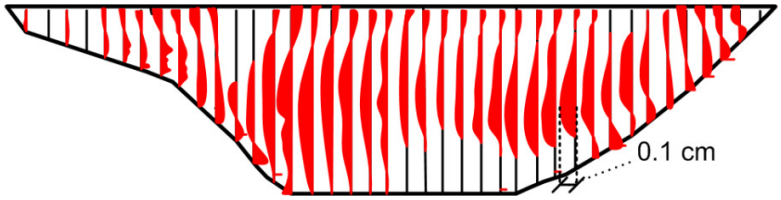

Figure 4.7 Face Plate Opening at the Maximum Reservoir Level

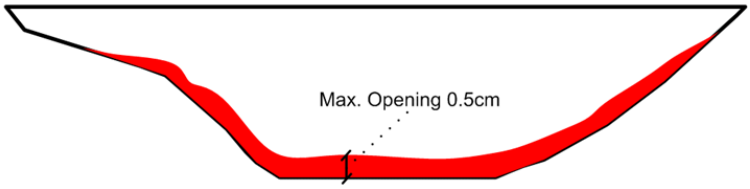

Figure 4.8 Opening from Plinth at the Maximum Reservoir Level

4.2 EFFECT of EARTHQUAKE LOADING on the ÇOKAL DAM

4.2.1 Seismic Loading on the Çokal Dam

Çokal Dam is located in a seismically critical region close to the active North Anatolian Fault. The design earthquake motion spectra and the time histories are

provided in Figure 4.9 for earthquake events with 144, 475, 975 and 2475 yr return periods (Askan and Öztürk, 2010). The return period of 144 yr is chosen as OBE event in accordance with national practice for Çokal Dam. After this event, the dam should be fully operational sustaining minimal damage. Maximum design earthquake (MDE) was chosen as the 2475 year return period earthquake. For the nonlinear transient time history analyses of the Çokal Dam, time histories that were response-spectrum matched to the target spectra were used. In Figure 4.9.c, the ground motions for different recordings (144, 475, 975 and 2475 yr) are presented. The PGA levels for these recordings are 0.28, 0.35, 0.45 and 0.6g's, respectively (Askan and Öztürk, 2010).

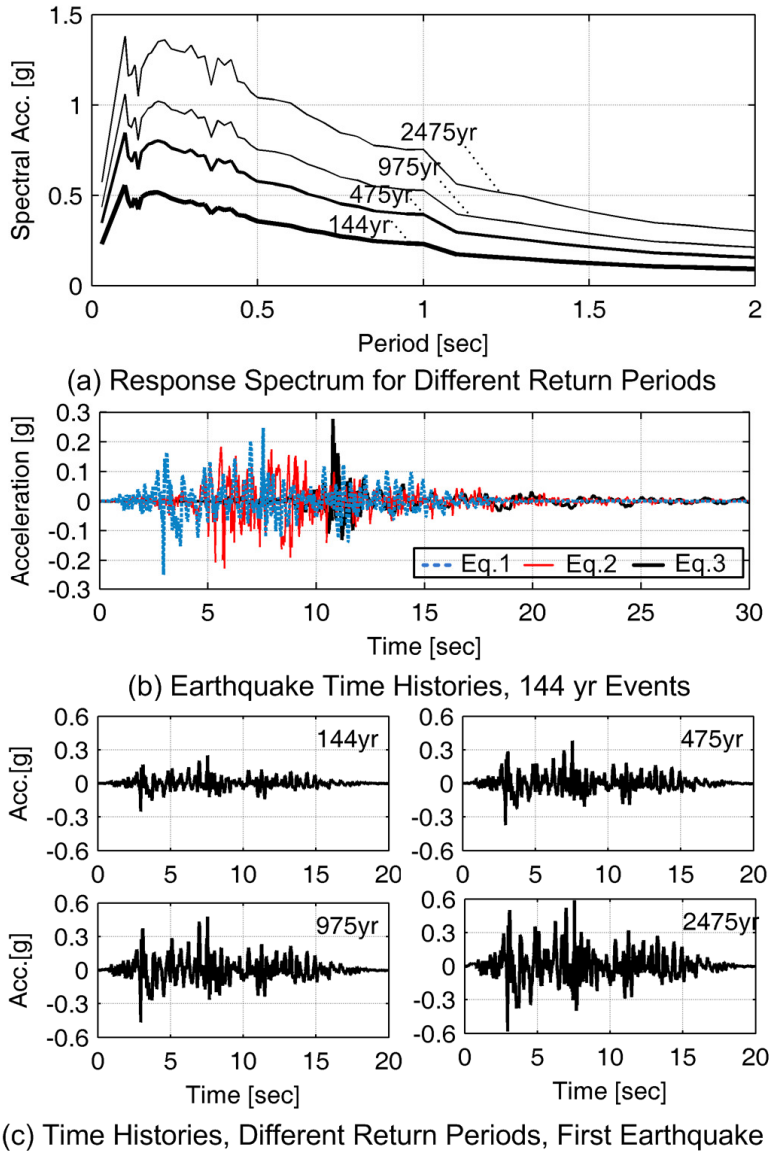

Figure 4.9 Earthquake Ground Motion Time Histories (Askan and Öztürk, 2010)

4.2.2 Results at the Maximum Cross-Section

The transient analyses of the Çokal Dam were performed using the 2 and 3D models for these design earthquakes. Horizontal and vertical motion at the crest of the dam is compared between 2D and 3D models and provided in Figure 4.10 for the 144, 475, 975 and 2475 yr events. The results for lateral motions are similar for both 2D and 3D analyses. Vertical motions are similar except for the time interval between 13^{th} and 20^{th} seconds for 475 yr event, 15^{th} and 20^{th} seconds for 975 yr event and 12^{th} and 18^{th} seconds for 2475 yr event.

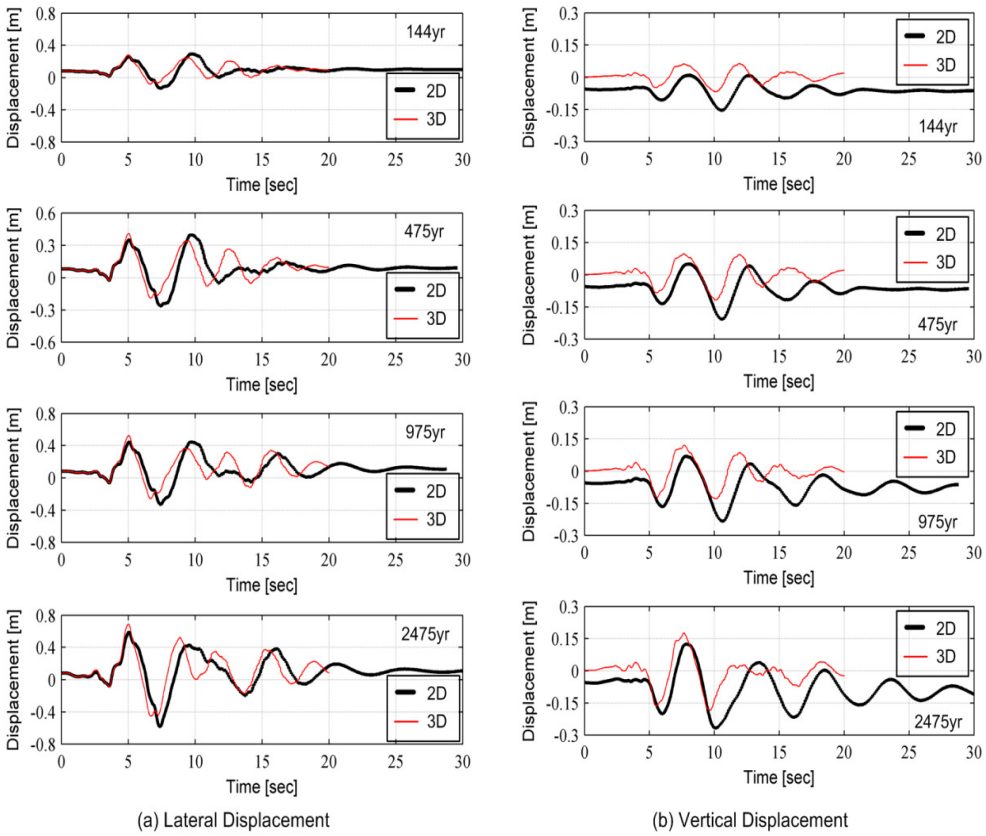

Figure 4.10 Comparison of Lateral and Vertical Displacement Time Histories for Different Earthquakes

In Figure 4.11, the comparison of the envelope of the shear strains in maximum cut section for 2 and 3D analysis are provided for all four events. The distribution of the shear strains near the upstream and downstream faces appear to be similar. The 3D model has a tendency of having smaller shear strains towards the embankment.

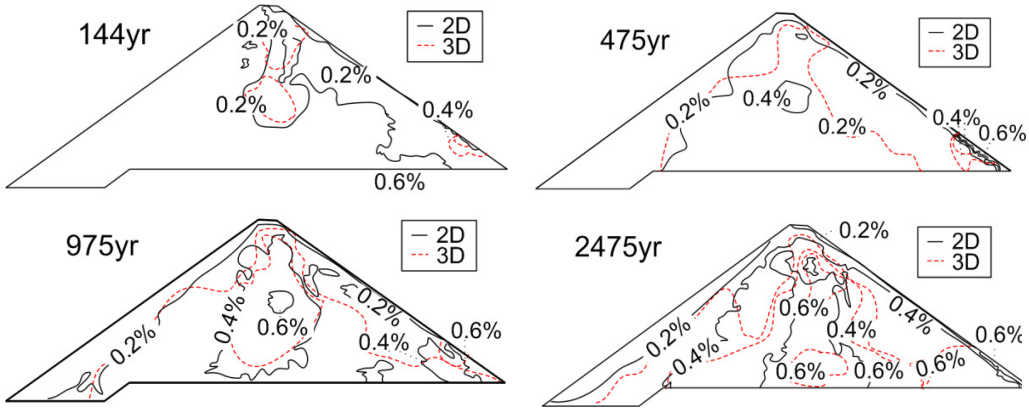

Figure 4.11 Comparison of The Envelope Shear Strains for Different Earthquakes

During earthquake excitation, axial stress distribution is an important component of the faceplate as it indicates the behavior of the faceplate. Extra tensile stresses were formed on the face plate along the whole length resulting to the spreading of the cracking from the bottom of the plate towards the dam crest, because of the effect of the ground motion. The alteration of the stresses along the faceplate at four nodes is represented in Figure 4.12. The 2 and 3D comparison sketches for 144,

475, 975 and 2475 yr earthquakes clearly define the formation of the tensile stresses and cracking on the faceplate between the elevations 43 and 61 m. Until the fifth second into the motion, the faceplate is capable of carrying the load applied to it according to its tensile strength limit; however, tensile strength of the concrete is exceeded after the fifth second leading to the plate cracking. The redistribution of the stresses within the concrete plate resulted in the reduction of stresses in the plate under this motion. Between elevations 9 and 26 m, stresses on the plate were zero. This region was already fully cracked after the impounding as given in the static analysis results for this load case.

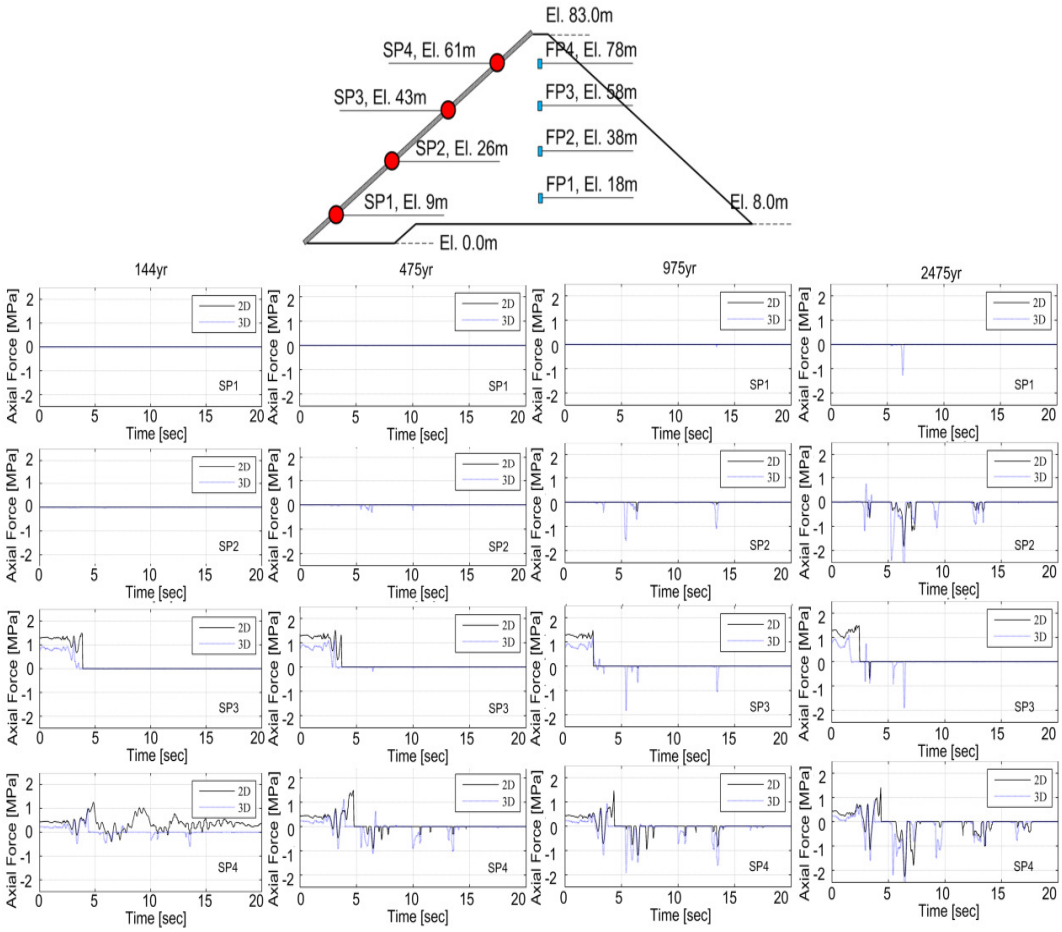

Figure 4.12 Variation of Axial Stress within the Face Plate for Different Earthquakes

The state of cracking on the face plate at the maximum cross-section is provided in Figure 4.13. For small events the results of 2 and 3D analyses are similar to each other. However, it can be seen that for larger events (975 and 2475 year return periods) the behavior at the mid height of the plates were different for 2 and 3D analyses. The effect of the valley ends cannot be represented for 2D model for these events.

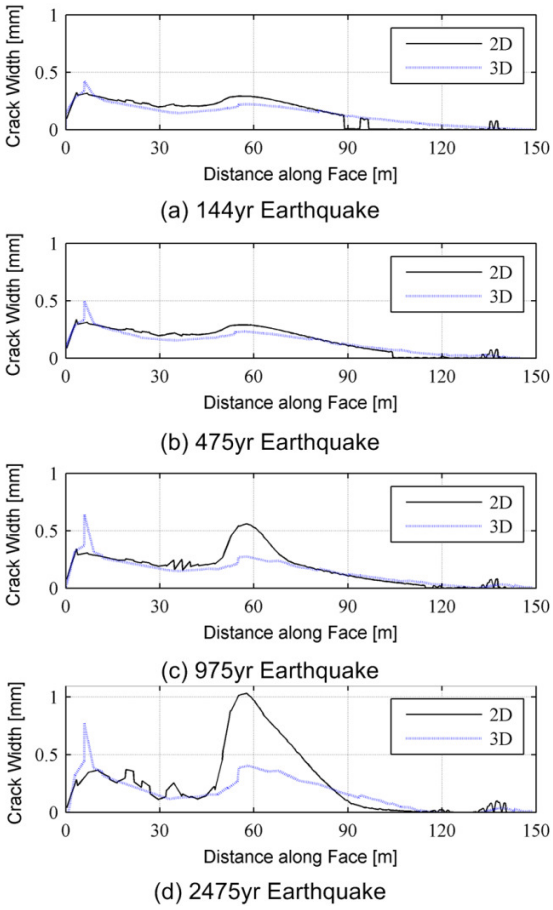

Figure 4.13 Crack-width on the Face Plate-Different Earthquakes

Furthermore, crack widths are larger for 2D model: 3D models do not follow the same trend. These results show that 3D model should be used to define the effects of the valley ends and to get more realistic results.

4.2.3 3D Effects

The contours of the crack widths on the face plate after the earthquakes with 144, 475, 975 and 2475 year return periods are presented in Figure 4.14. The cracking for the 144 and 475 year return period earthquakes are similar. For the 144 and 475 year low intensity earthquakes, maximum crack widths were limited to 0.4-0.5 mm spread to the base of the face plate. The 975 and 2475 year return period events are much more destructive for the faceplate with cracks spreading towards the crest of the dam. There are also some serious localized cracking: large cracks (>5cm) occurred at one location for the 975 yr earthquake and at two locations for the 2475 yr earthquake.

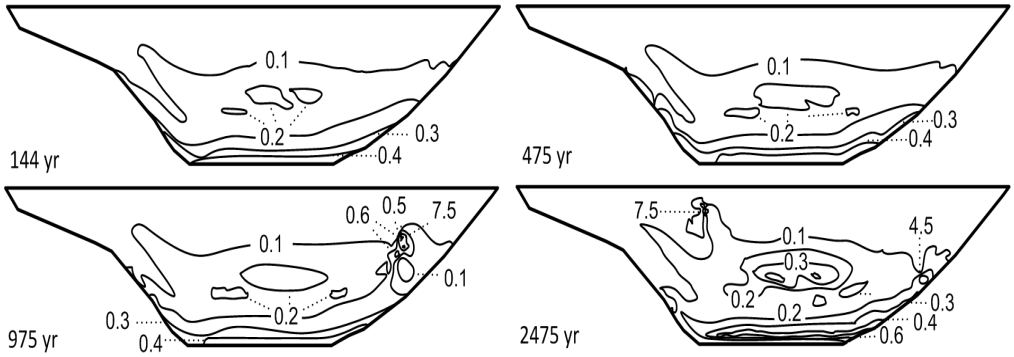

Figure 4.14 Contour of Crack width after the Earthquake (in mm)

The time history of the opening at the plinth for different locations along the face edges is provided in Figure 4.15 for the 144, 475, 975 and 2475 year return period events. During the strong ground motion period, the plinth opening increases returning to its former position after the strong motion. The maximum obtained for the 144 yr event was slightly larger than 1.0cm. For the 475 yr earthquake, again in the period of strong motion, plinth opened up about 1.5 cm's, later to end in pre-earthquake position. For the 975 and 2475 year return period earthquakes, plinth opening was 1.5 and 2.0 cm's, respectively. Moreover, for these earthquakes; the plinth suffers some residual opening. However, the difference of the positions before and after the earthquake did not appear to be large enough to cause a problem on the performance of the dam.

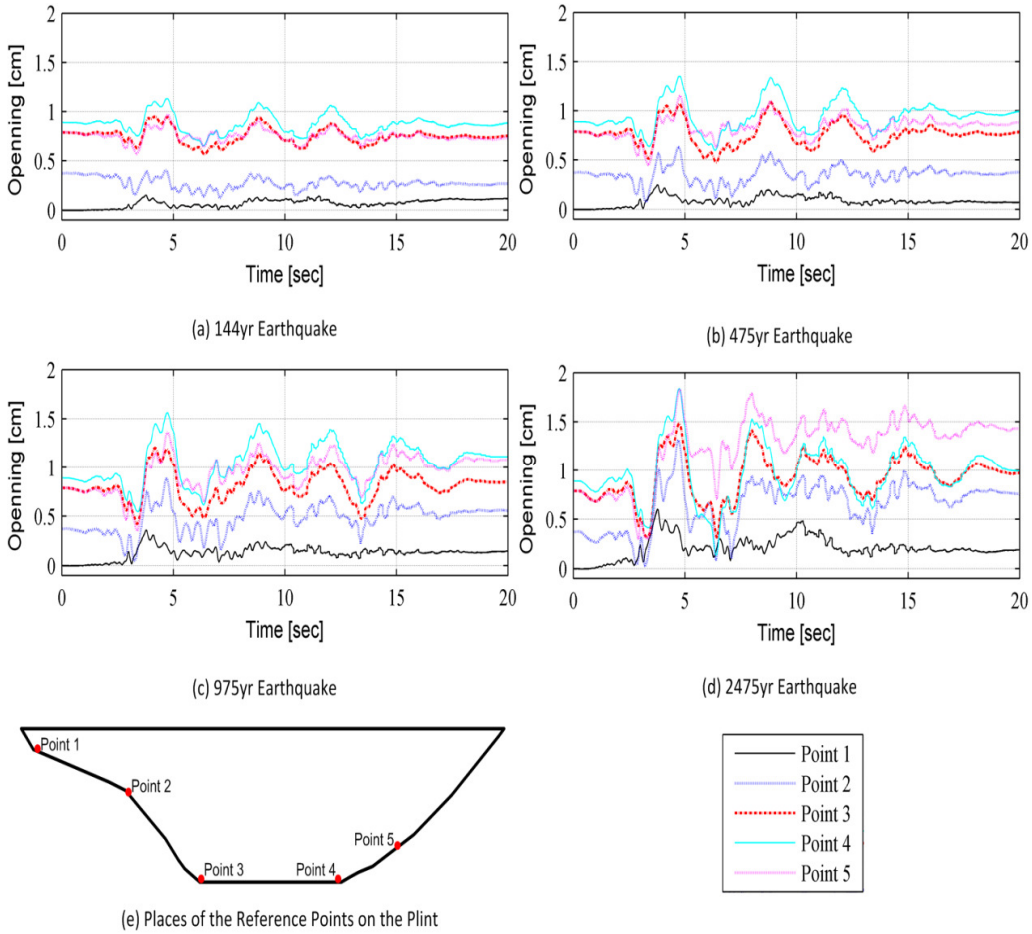

Figure 4.15 Time History of Plinth Opening at Different Locations around the Plate

The envelope of the maximum openings at the interface elements for the 144 and 2475 year return period earthquakes are provided in Figure 4.16.a. The opening after the end of the earthquake motion is provided in Figure 4.16.b. As given in the figures below, the construction joints opened very little during shaking in the 144 yr earthquake event. Many of the joints seem to be in a cycle of opening and closing during the ground motion with the maximum opening about 0.5 cm. At the end of the earthquake ground motion, most of the joints closed, permanent openings were observed only at the lower joints close to the valley sides. Smaller residual openings were obtained near the crest of the dam close to the mid-section (Figure 4.17). The envelope and the residual values of openings at the vertical construction joints were significantly larger for the 2475 year earthquake. Except for a region near the centre of the faceplate, nearly all vertical joints went through opening-closing cycles during the earthquake ground motion. Most of these joints closed at the end of the motion, except for the locations near the valley sides and at the dam crest. As mentioned before, there were two locations where the crushing of the face plate led to some large openings (about as large as 2.5 cm) in the vertical construction joints.

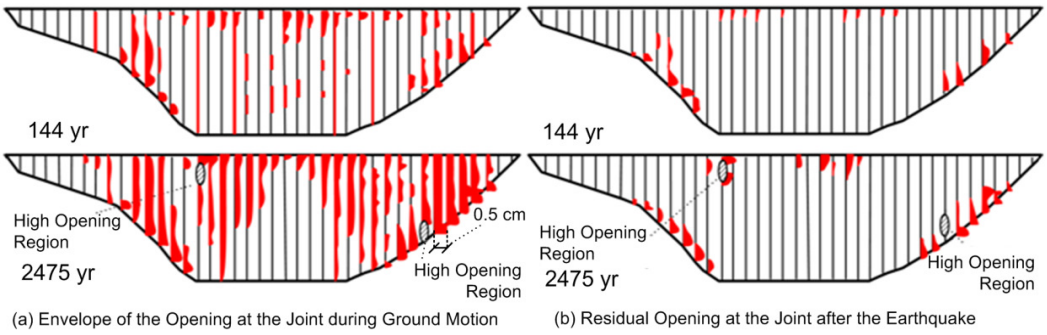

Figure 4.16 The Envelope and Residual of Maximum Opening at Interface Elements for Different Earthquakes

At the final state, for lower events (144 and 475 yr events), permanent openings are small and near the valley ends. However, for 975 yr event, except for a small region, permanent openings are less and near valley end as lower events. At 2475 year event, permanent openings occurred near the crest, valley ends with two high opening regions.

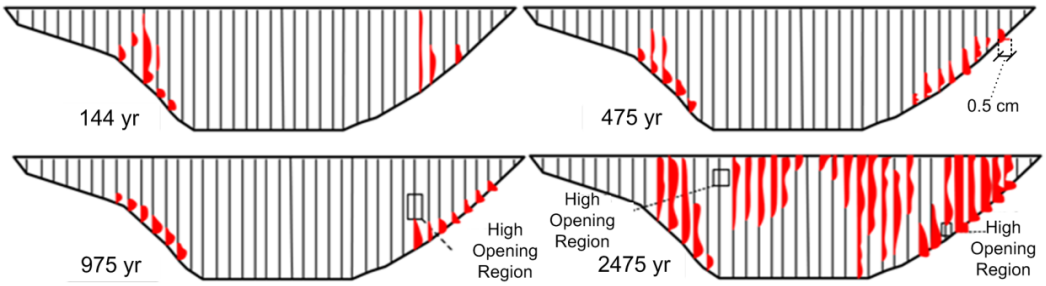

Figure 4.17 Final State of Opening on the Interface Elements for Different Earthquakes

The time history of the lateral opening at the interface where the maximum opening is obtained is provided below for the different earthquakes. The time history of joint opening at the location where the maximum opening is observed is provided in Figure 4.18. For the 144 year event, the opening at the joint changes between 2 and 3.5 mm and stays near 2.5 mm. However, for the 2475 year event, the behavior is different. The joint opening reaches 2.5 cm level abruptly, and oscillate around that level. This can be concluded to be as a result of the crushing of the plate near the joint observed at 5 second into the earthquake.

144yr 2475yr

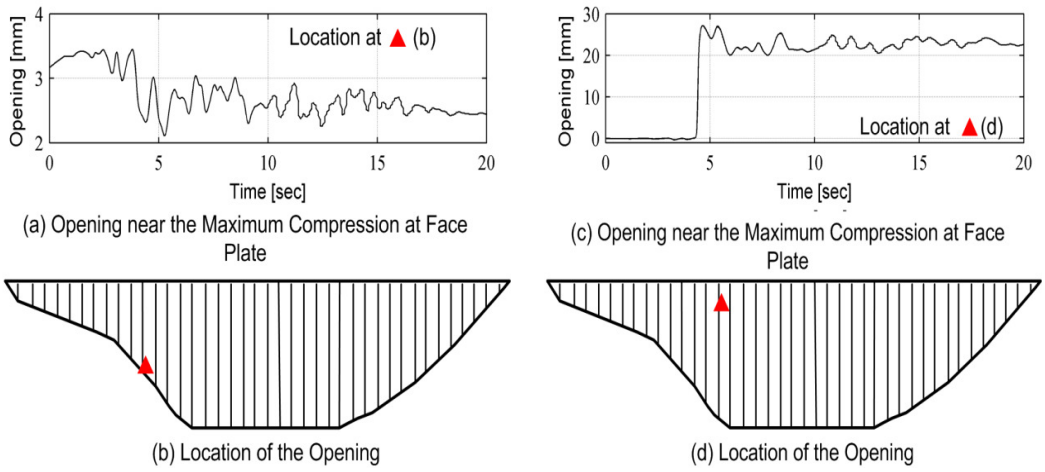

Figure 4.18 The Time History of Opening at Face Plate and Their Locations

The localized large cracking was obtained as a result of the crushing of the concrete at the locations provided in Figure 19.c, 19.d. Concrete compressive strength was exceeded at these locations. This is clearly defined in the time history of the compressive stress at these points as given in Figure 4.19. The maximum compressive stresses occurred at the localized maximum values of the crack widths obtained from Figure 4.19. The maximum compressive stress for the 144 yr earthquake was about 8 MPa obtained near the valley side, with the plate reverting to 6 MPa stress after the end of the earthquake shaking. On the other hand, a sudden increase in the face plate stress about 30 MPa was observed for the 2475 year return period event near the crest of the dam leading to the crushing of the plate at that location. The crushing resulted in a permanent damage on the face plate; the vertical construction joints were opened to a significant degree after the damage on the plate.

The time history of the lateral compression on the face plate at the location where the maximum compression on the plate is obtained is given below for the 144, 475, 975 and 2475 year return period earthquake events.

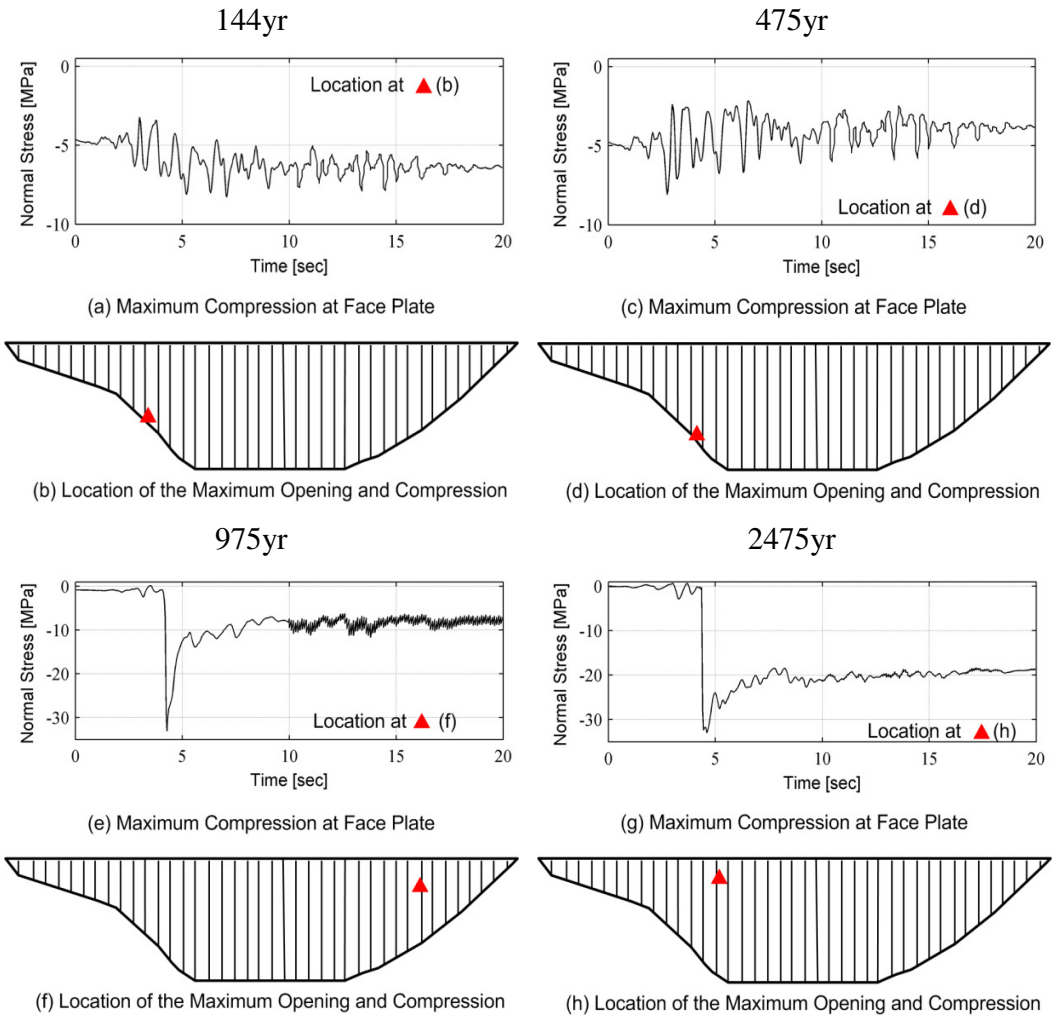

Figure 4.19 Time History of Lateral Compression for Different Earthquakes on the Face Plate

CHAPTER 5

SIMPLIFIED METHOD FOR PRELIMINARY DESIGN OF CFRD FACE PLATES

5.1 GENERAL

In developing countries, CFRDs have been increasing their popularity due to the advantages in construction and the lack of clayey materials. These dams are usually more economical. The design methodologies of such dams are based on empirical formulas based on past practice in the field. These formulas are used to calculate the thickness of the face plate and to estimate the crest settlement. However, recent poor experience in some dams (Chen and Han, 2009) has led to the reconsideration of the design methods and showed that field and laboratory investigations for these dams are crucial.

Academic studies, as conducted in previous chapters, are far from practical applications in preliminary designs of such systems. Using non-linear behavior in the calculations is very time consuming and is generally not-appropriate for a practicing manners. Simpler methods based on analytical detailed studies is hence necessary, to supplement the empirical formulas in the preliminary design. In this chapter, the detailed nonlinear analysis as given above will be used to obtain a much simpler analysis method to develop a simple methodology enabling the designer to control the cracking of the face plate.

5.2 METHODOLOGY

In order to design these structures, it is often necessary to use iterative calculations. Such iterative calculations, if conducted with detailed simulation models, would consume significant amount of time and may be counterproductive. Iterations are better conducted with practical methods, which should be in accordance with detailed simulations and be appropriate to the application. While detailed simulations, as carried above, require in depth knowledge of general purpose finite element programming and nonlinear material models, practical programs only require basic structural analysis background. Therefore, in order to develop the practical method, SAP2000 was used. The results from the proposed methodology, obtained by using linear finite element analysis program, were validated to the detailed analysis results obtained with general purpose finite element code DIANA.

The prediction of the crack width and the cracked region on the face plate is chosen as the purpose of the simplified method because the cracking region is critical to the seepage performance of the CFRD. Prediction of the crack length is done by reading the corresponding value of stress retrieved from the linear finite element analysis program, corresponding to the crack length that is pre-verified with detailed analysis as shown in Figure 5.1. The tensile stress value derived from Figure 5.1 is then divided to the tensile strength of the concrete to obtain Stress Ratio (*S.R.*) (Figure 5.2). Preliminary reinforcement ratio (ρ), concrete tensile strength (f_{ct}) and the tensile strength of reinforcement (f_y) were utilized to calibrate the formula (Equation 5.1) for the determining *S.R.* (Figure 5.2).

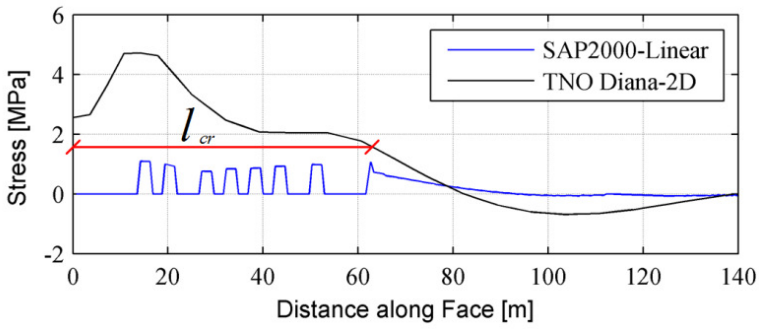

Figure 5.1 Stress Distribution along the Face Plate for Detailed Nonlinear and Linear Model

A number of analyses are conducted using both detailed simulations and finite element models in order to obtain the change of the stress ratio with respect to the design parameters. The material properties used in the analyses are provided in Table 5.1. These analyses, with varying material properties were used to obtain equation 5.1 defining a simple stress ratio for design purposes. The fit obtained using a linear assumption to the analyses results are presented in Figure 5.2.

$$S.R. = 0.74 + 4.6\frac{\rho f_y}{100 f_c} \tag{5.1}$$

where f_y is the yield strength of the reinforcement steel, f_c is the characteristic strength of the concrete, ρ is the reinforcement ratio and *S.R.* is the stress ratio to determine the crack region along the face plate.

Table 5.1 Material Types Used in Analyses

Modulus of Elastisity for Rockfill [MPa]	Modulus of Elastisity for Face-Plate [MPa]	Thickness of Face-Plate [m]	Compressive Strength of Conrete, f_c [MPa]	Tensile Strength of Conrete, f_c [MPa]	Reinforcement Ratio [%]
30	17000	0.5	13	1.3	0.3
30	20000	0.5	20	1.6	0.3
30	26000	0.5	30	1.9	0.3
30	30000	0.5	35	2.1	0.3
40	26000	0.5	30	1.9	0.3
40	30000	0.5	35	2.1	0.3
50	20000	0.8	20	1.6	0.3
50	26000	0.5	30	1.9	0.3
30	17000	0.3	13	1.3	0.6
40	17000	0.3	13	1.3	0.6
40	30000	0.3	35	2.1	0.6
40	17000	0.5	13	1.3	0.6
40	20000	0.5	20	1.6	0.6
50	17000	0.5	13	1.3	0.6
50	20000	0.5	20	1.6	0.6

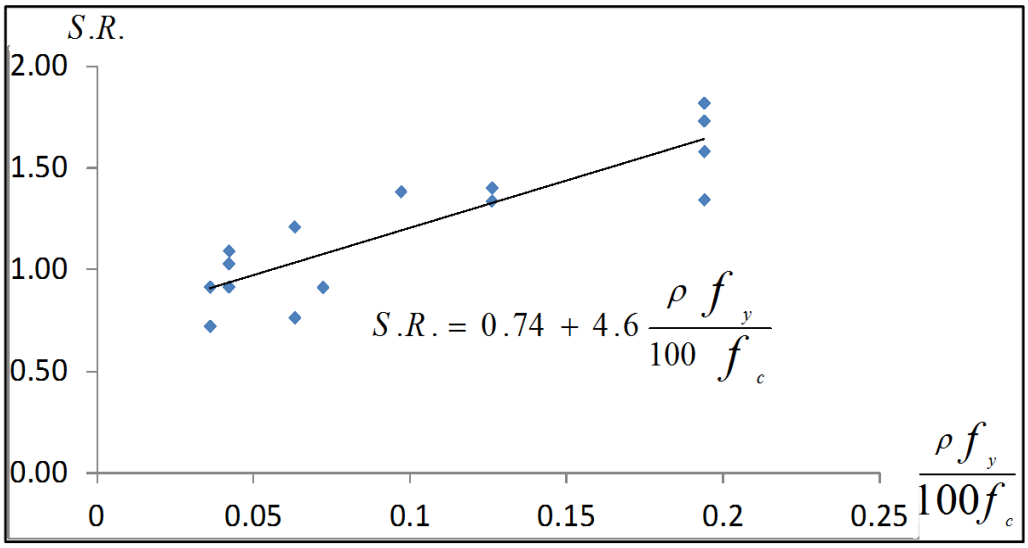

Figure 5.2 Determination of the Stress Ratio (S.R.) over Reinforcement Ratio, Yield Strength of Reinforcement and Characteristic Strength of Concrete (R^2=0.8)

The cracked length of the face plate is determined next. By multiplying the concrete tensile strength with this ratio (Equation 5.2), a threshold stress is determined. The location of this stress on the face plate, picked up from the tensile stress plot of the plate obtained from a simple analysis in SAP2000, provides the extent of cracking, i.e. the crack length (l_c). In Figure 5.3, the determination of this region is demonstrated.

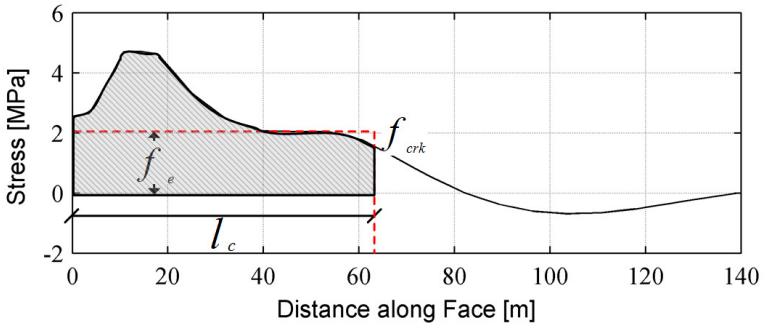

Figure 5.3 Determination of The Elastic Tensile Stress

$$f_{crk} = c\, f_{ct} \tag{5.2}$$

After this step, the elastic tensile stress is used to determine the crack width on the cracked region. As long as the conducted analyses are linear elastic, recommended ductility can be satisfied using this elastic tensile stress. Integrating the elastic stress in the cracked region, (Figure 5.3) and dividing the result to the crack length provides the average elastic tensile stress along the crack region (Equation 5.3).

$$f_e = \frac{\int_0^{l_c} \sigma \, dx}{l_c} \tag{5.3}$$

where f_{crk} is tensile stress obtained from the end of the crack region, f_{ct} is tensile strength of the concrete, f_e is average elastic tensile strength over crack region and l_c is the crack length.

In Figure 5.4, the calibration of maximum crack width with the corresponding elastic tensile strength over the tensile strength multiplied by reinforcement ratio is sketched. Equation 5.4 is obtained calibrating these parameters to the maximum crackwidth obtained from the detailed analyses. Crack limits of the concrete slabs are determined from the code of Turkish Standards (TS500). According to TS500, crack widths should be in the range of 0.1-0.4 mm. Large crack widths up to 0.5mm and up to 1mm were deemed acceptable by Mori (1999) and Haselsteiner and Ersoy (2011).

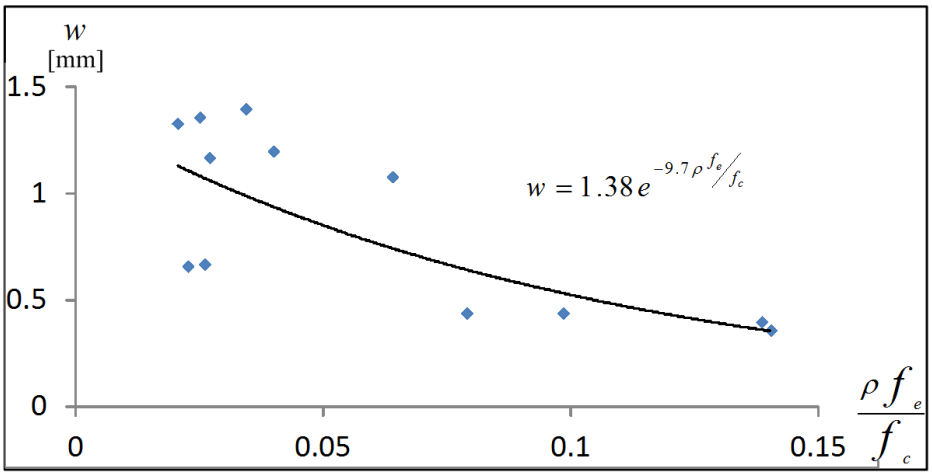

Figure 5.4 Determination of The Crack Width (R^2=0.7)

$$w = 1.38e^{-9.7\rho f_e/f_c} \text{ [mm]} \tag{5.4}$$

where w is the maximum crack width over the face plate.

The study given above can serve as guideline for the design of the face plate of a structure. The designer should first prepare a finite element model for the maximum cross section of the dam. In order to predict the tensile stresses that are obtained by the detailed analysis, rockfill should be taken into consideration in the mode(Figure 5.5). Using shell element in the fill model ensures the compatibility of the fill and the plate. Plinth contact can be modeled with compression only elements at the base of the model.

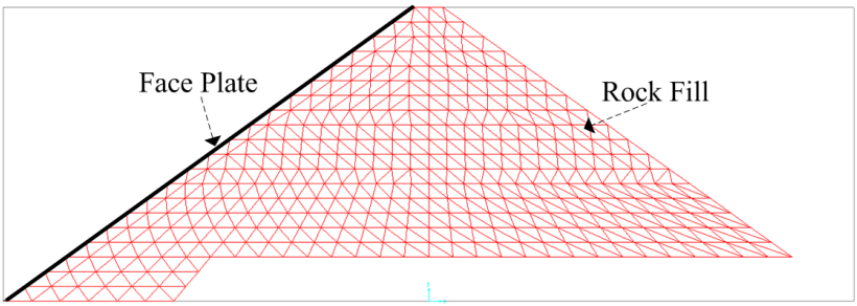

Figure 5.5 Linear Elastic Finite Element Model

Design of the face plate should be made at the MWL case. As seen previously, when the reservoir is at the MWL, the plate is under the most critical loading condition. The high tensile stresses on the plates lead to cracking on the face plate for the MWL. The designer should apply the forces that form under MWL case to the model. The designer should choose the modulus of elasticity (E_c), area (A_c) and the moment of inertia (I_c) of the concrete in the created model by a preliminary design.

The guidelines for reaching the final design of the face plate can be summarized as follows;

1) The elasticity modulus, the cross sectional area and moment of inertia of the concrete member and the elasticity modulus of the rockfill should be determined.
2) Simple 2D linear finite analyses are conducted.
3) Then, S.R. as given in Equation 5.1 is decided.
4) After determination of the *S.R.*, cracked region and its length should be determined implying the "critical zone".
5) Average elastic tensile stress of the member in the critical zone can be calculated by Equation 5.3.
6) Crack width can be found based on the average elastic tensile stress by Equation 5.4.
7) If crack width is out of the selected range, then the initial parameters that are defined at step 1 should be changed and procedure should be repeated. If crack width is within the acceptable range, then preliminary design can be terminated.

In conclusion, a simplified elastic analysis can be used on the maximum cross section of the CFRD to limit the cracking on the face plate as given above. The procedure given above is calibrated to numerous nonlinear detailed nonlinear analyses. Because of its approximate nature, it is suggested to be used for pre-design only.

CHAPTER 6

CONCLUSION

6.1 SUMMARY

In this study, the performances of concrete faced rockfill dams are investigated for static and seismic loading conditions. 2D and 3D approaches to the modeling of CFRDs were investigated and compared. The evolution, current trends and characteristics of CFRDs, the strength characteristics of the CFRDs, the constitutive laws used for the modeling of CFRDs were presented in second chapter. Gradation of rockfill materials, the softening and loss of strength occurring under earthquake motions and the effect of the face plate are the determining factors on the integrity of the CFRDs. Analysis technique is another major issue for CFRDs. Reinforced concrete face plate, rockfill and the interface between the fill and the concrete plate need to be modeled with the relevant constitutive models. In this study, rockfill, the interface between the rockfill and the face plate and the face plate were simulated using detailed nonlinear models which were calibrated to define the component behavior using experimental data. In forth chapter, the simulations conducted for evaluating the performance of the chosen case study, the Çokal Dam, is presented. The analysis covers the impounding and the earthquake loading of the Çokal CFRD. CFRD deformation during impounding and earthquake loading depends on intact particle strength, rockfill gradation, mineralogy, foundation conditions as well as construction technique and loading. 2 and 3D analyses were conducted and compared for the impounding stage and the earthquake loading. The

results from 2 and 3D analyses compared well, moreover, behavioral aspects of a CFRD, that cannot be obtained using a 2D analyses, such as stress distribution within the plate, crack width distribution along the face slab, the interactions of the face plate strips were obtained in the 3D analyses..In the fifth chapter, a study aimed at developing a practical guideline for face plate design was presented. The suggested procedure was prepared comparing and calibrating the results of detailed 2D analysis models and simple linear elastic 2D models. By conducting a relatively simple 2D analysis, the designer can assess the choices of materials for the selected design goals instead of depending on former practice or empirical methods. However, as higher CFRDs are built, the face plate stresses become more critical and are heavily affected by the condition and construction of the fill. Therefore, above the height of 100m, a detailed analysis is suggested to the designer for avoiding performance issues with the dam during the operation stage.

6.2 CONCLUSIONS

The conclusions from this study are given below:

- For the impounding stage of the reservoir, the displacements of fill were obtained very similar from the 2 and 3D analyses. According to the analyses, the impounding of the reservoir changes the state of stress relatively significantly only near the upstream face of the dam.
- The effect of the valley sides reduces the displacements of the dam body to some extent. However, on the middle strip of the face plate, the stresses and the cracking on the face plate for the 2 and 3D models agree well.
- When the reservoir is empty, face plate is under compression and compression is increasing towards the plinth. During the impounding, tensile stresses are

generated slowly on the face plate. At MWL, the face plate is completely under tensile stress.

- The problem of the leakage on the faceplate of CFRDs at the impoundment and operation stage is due to the cracking of the faceplates. For the given case study, about 30% percent of the faceplate was estimated to be cracked with an average crack-width of 0.4 mm up to 1 mm.
- Horizontal cracks forming parallel to the main axis of the dam (opening in up-down direction) are the main cracks observed at the MWL. Vertical cracking is only observed, with very small crack widths (less than 0.1mm), at the edges of the faceplate boundaries near the valley sides.
- After the earthquake loading, cracks lead their way upwards from plinth to crest of the dam. For low return period events this extension is minor; on the other hand, for the 975 and 2475 year return period events, much larger crack widths are observed.
- 2 and 3D models for evaluating the performance of CFRDs was compared in this study. As expected, the effect of side valleys can only be seen on 3D models which indicate the cracks occurred along the faceplate away from maximum cross section. The spatial distribution of cracking and stresses on the face plate can only be observed in the 3D model as well. Finally, the 3D model has the advantage of showing the interaction of the face plate strips during an earthquake motion.
- The 975 and 2475 year return period events are important for the cracks spreading on the faceplate, as well as for formation of localized cracking on the plate. The 3D analyses showed plate strips hitting each other at some locations to lead to local crushing on the face plate. Serious localized crushing occurs (>5cm) at one location for the 975 yr earthquake and at two locations for the 2475 yr earthquake 3D analyses predicted smaller lateral cracking compared to the 2D results on the maximum cross section for the high return

period events. However, the crushing of the face plate strips are predicted to be the real issue with the face plate undergoing severe damage at crushing locations at the interfaces. This behavior closely resembles the performance observed in the ZipingPu CFRD in the 2008 Wenchuan earthquake. A simple method using the determination of the crack width on the face plate to lead to face plate design parameters is proposed. The aim of this study is to provide the designer with a relatively easier analysis approach to determine the face plate thickness, reinforcement ratio and concrete quality. The simplified method proposed was calibrated to the detailed analyses conducted during the scope of this study. Practical use of limited analysis and simple finite element codes enable the method to be used quickly for pre-design. This method is thought to be applicable up to 100 m high dams: for higher systems, plate cracking is a significantly complex issue requiring in depth analyses. Detailed nonlinear modeling is necessary for such structures.

CFRD dams are complex structures. While the performance prediction and the simulation presented in this study for the Çokal Dam agree with the observations for a range of dams, different boundary conditions, construction techniques and loading conditions can lead to a different performance condition. Therefore, the results presented here should not be accepted to be literally valid for all CFRDS.

6.3 SUGGESTIONS AND FUTURE RESEARCH

Abrupt changes of the stresses at the localized areas on the face plate for higher return period earthquakes was shown to result in the crushing of face plate concrete in chapter 4. Such crushing was observed on the ZipingPu Dam which is the only CFRD to undergo a very severe earthquake motion upto now. The solution for

the crushing of concrete at these regions could be increasing the thickness of the face plate or increasing of the face plate concrete strength, which are equally expensive measures. The damage on the plate can also be repaired after the earthquake event. For this purpose, grouting, epoxy treatment or geomembranes could be used. For applying these treatment options the dam may need to be drawn down, which is a significant disadvantage for reservoirs taking a long period to fill completely.

Cracking of the face plate appears to be a significant issue for long-term operation of these systems. Accordingly, corrosion-resistant reinforcement with protective covering is advised to be used in the face plates. The diminutive cracks as such may not lead to much seepage from the dam, however, reservoir water with significant corrosive content is bound to enter the face plate and reach the reinforcements.

Seepage into the CFRD fills and its effects is one of the future research areas that should be conducted to understand and predict the performance of these dams better. For large projects with large reservoirs, the prediction of seepage correctly correlated to cracking on the face plate may prevent the enormous costs that are incurred by repairing the face plate after the impounding.

Another important future research area is the effect of long-term settlements on the face plate and the fill performance. Most of these systems show settlements increasing with time with a decreasing rate, stabilizing usually after 10's of years. The effect of such deformation on the face plate needs to be investigated.

Simplified methods for the preliminary design of these systems need further investigation. More case studies with different fill characteristics should be included in such an investigation to reach a broad conclusion and a more established methodology. The case study and the analyses conducted in this thesis should be regarded as limited in scope.

REFERENCES

ACI Committee 318. "*Building Code Requirements for Structural Concrete and Commentary 2005.*", American Concrete Institute, 2004.

Arici, Y. *"Investigation of the cracking of CFRD face plates*.", In: *Comput Geotech, Vol. 38, pp. 905-916*, 2011.

Askan, A., Ozturk, N. "*Seismic Hazard Study for Cokal Dam*.", Earthquake Engineering Research Center, METU, Ankara, 2010.

Boulanger, R.W., Bray, J.W., Merry, S.M., Mejia, L.H. "*Three-dimensional dynamics reponse analyses of Cogswell Dam*.", In: *Can Geotech, Vol. 32, pp. 452-464*, 1995.

Cao, X., He, Y., Xiong, K. *"Confining pressure effect on dynamic response of high rockfill dam."* In: Front *Arch Civil Engineering, China, Vol. 4, Issue 1, pp. 116–126*, 2010.

Chen, S.S., Han, H.Q. "*Impact of the '5.12' Wenchuan earthquake on ZipingPu concrete face rockfill dam and its analysis*.", In: *Geomechanics and Geoengineering, Vol. 4, Issue 4, pp. 299-306*, 2009.

Cooke, J.B. *"Progress in Rockfill Dams.", (18th Terzaghi Lecture).* In: *Geotech. Engrg., ASCE, Vol. 110, Issue 10, pp. 1381-1414*, 1984.

Cooke, J.B., and Sherard, J. L. "*Concrete-Face Rockfill Dam: II. Design*", In: *Geotech. Engrg., ACSE, Vol. 113, Issue 10, pp. 1113-1132,* 1987.

Feenstra, P.H., Rots, J.G., Arnesen, A., Teigen, J.G., Høiseth, K.V. (edited by de Borst et al.) "*A 3D constitutive model for concrete based on a co-rotational concept.",* In: *EURO-C 1998, Computer Modeling of Concrete Structures. Rotterdam: Balkema., The Netherlands, pp. 13–22,* 1998.

Feng, D., Zhang, G., Zhang, J. "*Three-dimensional seismic response analysis of a concrete-faced rockfill dam on overburden layers*." In: *Frontiers of Architecture and Civil Engineering in China, Vol. 4, Issue 2, pp. 258-266,* 2010.

Gazetas, G. *"Seismic response of earth dams: some recent developments.",* In: *Soil Dyn Earthquake Eng, Vol. 6, Issue 1, pp. 2-47*, 1987.

Gergely, P., Lutz, L.A. (edited by Philleo, R.E.) "*Maximum crack width in reinforced concrete flexural members."* In: *Causes, Mechanism and Control of Cracking in Concrete , Detroit: American Concrete Institute, Vol 20, pp. 87-117,* 1968.

Groen, A.E. "*Elastoplastic modelling of sand using a conventional model.*" In: *Tech Rep 03.21.0.31.34/35,* Delft University of Technology, 1995.

Hacıefendioğlu, K., Bayraktar, A., Başağa, H.B. "*Estimation of stochastic nonlinear dynamic response of rock-fill dams with uncertain material parameters for non-stationary random seismic excitation*." In: *Springer, Vol. 61, pp. 43-55*, 2007.

Haselsteiner, R., Ersoy, B. (edited by Pina et al.) "*Seepage Control of Concrete Faced Dams with respect to Surface Slab Cracking."* In: *6th International Conference on Dam Engineering, Lisbon, Portugal, February 15-17*, 2011

Johannesson, P. and Tohlang, S.L. "*Lessons learned from Mohale. International Water Power and Dam Construction"* URL: http://www.waterpowermagazine.com (Accessed 29/03/2011).

Kramer, S.L. *"Geotechnical Earthquake Engineering"*, Prentice Hall, 1996.

Kong, X., Liu, J. "*Dynamic Failure Numeric Simulations of Model Concrete-Faced Rock-Fill Dam.*", 2002.

Mori, R.T. "*Deformation and Cracks in Concrete Face Rockfill Dams. Proceedings, Second Symposium on Concrete Face Rockfill Dams."* In: *Brazilian Committee on Dams, Florianopolis, Brazil, pp. 49-61*, 1999.

Özkan, M.Y. "*A review of considerations on seismic safety of embankments and earth and rock-fill dams."* In: *Elsevier, Vol. 17, pp. 439-458*, 1998.

Peck, R.B. "*Where has all the Judgement Gone"* In: *Fifth Laurits Bjerrum Memorial Lecture*, National Research Council of Canada, 1980.

Pinto, N.L.S. "*A challenge of very high CFRD dams: Very high concrete face compressive stresses."* In: *5th International Conference on Dam Engineering*, Lisbon, Portugal., 2007.

SAP2000. *"CSI Analyses Reference Manual for SAP2000, ETABs and SAFE."* Computers Structures, Inc., Berkeley, California, USA, 2009.

Seed, H.B., Wong, R.T., Idriss, I.M., Tokimatsu, K. "*Moduli and Damping Factors for Dynamic Analysis of Cohesionless Soils."*. EERC, Berkeley, California, Rep No: 84/14, 1984.

Singh, B., and Varshney, R.S. "*Engineering For Embankment Dams*", A.A. Balkema Publishers, Brookfield, 1995.

Sobrinho, J.A., Xavier, L.V., Albertoni, C., Correa, C., Fernandes, R. "*Performance and concrete repair at Campos Novos."* In: *Hydropower Dams, Vol. 2*, 2007.

TNO DIANA., 2008."*User's Manual R. 9.3*."

TS500, 2000."*Requirements for Design and Construction of Reinforced Concrete Structures.*" Turkish Standards Institution (TSE).

Uesugi, M., Kishida H., Uchikawa, Y. "*Friction between dry sand and concrete under monotonic and repeated loading."* In: *Soils Found, Vol. 30, Issue 1, pp. 115-128*, 1990.

Varadarajan, A., Sharma, K.G., Venkatachalam, K., Gupta, A.K. "*Testing and modeling two rockfill materials."* In: *Geotech Geoenv Eng, Vol. 129, Issue 3, pp. 206–218*, 2003.

Vermeer, P.A., De Borst, R. "*Non-associated plasticity for soils, concrete and rock."* In: *Heron, Vol. 29, Issue 3, pp. 3-64*, 1984.

Zhang, G., Zhang, J.M. "*Numerical modelling of soil-structure interface of a concrete face rockfill dam."* In: *Comput Geotech, Vol. 36, Issue 5, pp. 762–772*, 2009.

Zhang, G., Zhang, J.M., Yu, Y. "*Modeling of gravelly soil with multiple lithologic components and its application."* In: *Soils Foun, Vol. 47, Issue 4, pp. 799-810*, 2007.